Membrane Bound O-Acyltransferase 7 (MBOAT7) Shapes Lysosomal Lipid Homeostasis and Function to Control Alcohol-Associated Liver Injury.

Venkateshwari Varadharajan[1,3,6], Iyappan Ramachandiran[1,3,6], William J. Massey[1,3,6], Raghav Jain[9], Rakhee Banerjee[1,3,6], Anthony J. Horak 3rd[1,3,6], , Megan R. McMullen[4,6], Emily Huang[4,6], Annette Bellar[4,6], Shuhui W. Lorkowski[2], Kailash Guilshan[10], Robert N. Helsley[11], Isabella James[9], Vai Pathak[4,6], Jaividhya Dasarathy[6,7], Nicole Welch[4,6], Srinivasan Dasarathy[3,4,6], David Streem[8], Ofer Reizes[2,3], Daniela S. Allende[5,6], Jonathan D. Smith[1], Judith Simcox[9], Laura E. Nagy[3,4,6], and J. Mark Brown[1,3,6,#]

[1]Department of Cancer Biology, Lerner Research Institute of the Cleveland Clinic, Cleveland, OH, USA
[2]Department of Cardiovascular and Metabolic Sciences, Lerner Research Institute of the Cleveland Clinic, Cleveland, OH, USA
[3]Center for Microbiome and Human Health, Lerner Research Institute, Cleveland Clinic, Cleveland, OH, USA
[4]Department of Inflammation and Immunity, Lerner Research Institute, Cleveland Clinic, Cleveland, OH, USA
[5]Department of Anatomical Pathology, Cleveland Clinic, Cleveland, OH, USA
[6]Northern Ohio Alcohol Center (NOAC), Lerner Research Institute, Cleveland Clinic, Cleveland, OH, USA
[7]Department of Family Medicine, Metro Health Medical Center, Case Western Reserve University, Cleveland, OH, USA
[8]Lutheran Hospital, Cleveland Clinic, OH, USA
[9]Department of Biochemistry, University of Wisconsin-Madison, Madison, WI, USA
[10]Center for Gene Regulation in Health and Disease (GRHD), Cleveland State University, Cleveland, OH, USA
[11]Department of Pharmacology & Nutritional Sciences, Saha Cardiovascular Research Center, University of Kentucky College of Medicine, Lexington, KY, USA

[#] = To whom correspondence should be addressed: Department of Cardiovascular and Metabolic Sciences, Cleveland Clinic, Cleveland, OH 44195, USA. Tel: 216-444-8340; Fax: 216-444-9404; E-mail: brownm5@ccf.org

Running Title: Hepatocyte MBOAT7 Suppresses Alcohol-Associated Liver Disease

Key Words: hepatology, alcohol-associated liver disease, gastroenterology, metabolism

Abbreviations used: AA, arachidonic acid; ALD, alcohol-associated liver disease; ASO, antisense oligonucleotide; BMP, bis(monoacylglycerol)phosphate; Cer, ceramide; CL, cardiolipin; DAG, diacylglycerol; GWAS, genome wide association studies; LPI, lysophosphatidylinositol; LPIAT1, lysophosphatidylinositol acyltransferase 1; *MBOAT7,* membrane-bound O-acyltransferase 7; *Mboat7*^{HSKO}, *Mboat7* hepatocyte-specific knockout mice; *Mboat7*^{MSKO}, *Mboat7* myeloid-specific knockout mice; NAFLD, non-alcoholic fatty liver disease; PA, phosphatidic acid; PC, phosphatidylcholine; PE, phosphatidylethanolamine; PG, phosphatidylglycerol; PI, phosphatidylinositol; PS, phosphatidylserine; PUFA, polyunsaturated; TAG, triacylglycerol.

Abstract

Several recent genome-wide association studies (GWAS) have identified single nucleotide polymorphism (SNPs) near the gene encoding membrane-bound *O*-acyltransferase 7 (*MBOAT7*) that is associated with advanced liver diseases. In fact, a common *MBOAT7* variant (rs641738), which is associated with reduced *MBOAT7* expression, confers increased susceptibility to non-alcoholic fatty liver disease (NAFLD), alcohol-associated liver disease (ALD), and liver fibrosis in those chronically infected with hepatitis viruses B and C. The *MBOAT7* gene encodes a lysophosphatidylinositol (LPI) acyltransferase enzyme that produces the most abundant form of phosphatidylinositol 38:4 (PI 18:0/20:4). Although these recent genetic studies clearly implicate MBOAT7 function in liver disease progression, the mechanism(s) by which MBOAT7-driven LPI acylation regulates liver disease is currently unknown. Previously we showed that antisense oligonucleotide (ASO)-mediated knockdown of *Mboat7* promoted non-alcoholic fatty liver disease (NAFLD) in mice (Helsley et al., 2019). Here, we provide mechanistic insights into how *MBOAT7* loss of function promotes alcohol-

associated liver disease (ALD). In agreement with GWAS studies, we find that circulating levels of metabolic product of MBOAT7 (PI 38:4) are significantly reduced in heavy drinkers compared to age-matched healthy controls. Hepatocyte specific genetic deletion (*Mboat7*^{HSKO}), but not myeloid-specific deletion (*Mboat7*^{MSKO}), of *Mboat7* in mice results in enhanced ethanol-induced hepatic steatosis and high concentrations of plasma alanine aminotransferase (ALT). Given MBOAT7 is a lipid metabolic enzyme, we performed comprehensive lipidomic profiling of the liver and identified a striking reorganization of the hepatic lipidome upon ethanol feeding in *Mboat7*^{HSKO} mice. Specifically, we observed large increases in the levels of endosomal/lysosomal lipids including bis(monoacylglycero)phosphates (BMP) and phosphatidylglycerols (PGs) in ethanol-exposed *Mboat7*^{HSKO} mice. In parallel, ethanol-fed *Mboat7*^{HSKO} mice exhibited marked dysregulation of autophagic flux and lysosomal biogenesis when exposed to ethanol. This was associated with impaired transcription factor EB (TFEB)-mediated lysosomal biogenesis and accumulation of autophagosomes. Collectively, this works provides new molecular insights into how genetic variation in *MBOAT7* impacts ALD progression in humans and mice. This work is the first to causally link MBOAT7 loss of function in hepatocytes, but not myeloid cells, to ethanol-induced liver injury via dysregulation of lysosomal biogenesis and autophagic flux.

Introduction

End stage liver diseases account for approximately 2 million deaths annually worldwide, with nearly half of liver disease-associated deaths arising from complications of alcohol-associated and non-alcoholic fatty liver disease (NAFLD)-related cirrhosis, and the other half driven by viral hepatitis and hepatocellular carcinoma. It is generally appreciated that there are some shared mechanisms driving liver injury from viral, NAFLD, or alcohol-associated liver disease (ALD)-driven etiologies, but also etiology-specific drivers that uniquely shape the

91 pathogenesis of liver failure. Although there has been great progress in identifying the "multiple
92 hits" that lead to end stage liver disease, we are only beginning to understand the cellular and
93 molecular mechanisms driving etiology-specific liver disease progression. Within the evolving
94 "multiple hit" theory of liver disease progression, it is clear that interactions between
95 environmental factors (i.e. diet, microbiome, alcohol, viral infection, environmental toxins, etc.)
96 and genetic determinants uniquely contribute to liver injury (Cohen et al., 2011; Rinella and
97 Sanyal, 2016). Currently, the only option for end-stage liver disease is liver transplantation.
98 However, the availability of viable donor livers is finite, and pharmacological approaches to
99 improve outcomes are simply lacking due to our poor understanding of the underlying
100 mechanisms of disease pathogenesis. Given this, there is a clear need to understand the
101 genetic and environmental interactions promoting the progression of liver disease from simple
102 steatosis to more advanced inflammatory and fibrotic disease. We address this gap here by
103 investigating the mechanisms linking a recently identified liver disease susceptibility gene in
104 combination with alcohol exposure.

105 Genome-wide association studies (GWAS) provide a powerful unbiased tool to identify new
106 genes contributing to human disease, allowing for pinpoint accuracy in identification of new
107 potential drug targets. This is exemplified by the recent success story of GWAS discoveries
108 leading to rapid development of monoclonal antibodies targeting proprotein convertase
109 subtilisin/kexin type 9 (PCSK9) for hyperlipidemia and cardiovascular diseases (Sabatine MS
110 2019). Since 2015, several independent GWAS studies have identified a liver disease
111 susceptibility locus (rs641738) near the genes encoding *MBOAT7* and *TMC4* (Buch et al.,
112 2015; Mancina et al. 2016; Vitasalo et al., 2016; Krawczyk et al., 2017; Thabet et al., 2016;
113 Thabet et al., 2017; Teo et al., 2021). It is important to note that the rs641738 T-allele (~43%
114 allele frequency in European ancestry populations) is associated with all major forms of liver

115 injury including NAFLD, alcohol associated-liver disease (ALD), and viral hepatitis-induced
116 fibrosis (Buch et al., 2015; Mancina et al. 2016; Vitasalo et al., 2016; Krawczyk et al., 2017;
117 Thabet et al., 2016; Thabet et al., 2017; Teo et al., 2021). The rs641738 variant is associated
118 with a C > T missense single nucleotide polymorphism (SNP) within the first exon the *TMC4*
119 gene, but the GTEx project shows that *TMC4* is not abundantly expressed in human liver (1.4
120 transcripts per million).We previously showed that mice lacking *Tmc4* (*Tmc4*$^{-/-}$) have normal
121 high fat diet-induced hepatic steatosis (Helsley et al., 2019). We also recently demonstrated
122 that antisense oligonucleotide (ASO)-mediated knockdown of *Mboat7* promotes insulin
123 resistance, hepatic steatosis, hepatocyte death, inflammation, and early fibrosis in high fat diet-
124 fed mice (Helsley et al., 2019). In parallel, four independent groups also showed that *Mboat7*
125 loss of function promotes hepatic steatosis, inflammation, and fibrosis in mice (Meroni et al.,
126 2020; Tanaka et al., 2021; Thangapandi et al., 2021; Xia et al., 2021). Collectively, *MBOAT7* is
127 a genetic determinant of advanced liver disease, but how this gene shapes susceptibility to
128 environmental cues is still an area of intense investigation.

129 The *MBOAT7* gene encodes a lysophospholipid acyltransferase enzyme (also known as
130 lysophosphatidylinositol acyltransferase 1, LPIAT1), which uniquely contributes to the Land's
131 cycle of membrane phospholipid remodeling (Shindou and Shimizu 2009). The Land's cycle is
132 a series of phospholipase-driven deacylation and lysophospholipid acyltransferase-driven
133 acylation reactions that shape membrane asymmetry and diversity (Shindou and Shimizu
134 2009). It is important to note that MBOAT7 selectively diversifies the fatty acid composition of
135 membrane phosphatidylinositol (PI) species and not phospholipids with other head groups and
136 exhibits acyl chain specificity for polyunsaturated fatty acids (Shindou and Shimizu, 2009;
137 Gijón et al., 2008; Zarini et al., 2014; Caddeo A., et al., 2019; Caddeo A., et al. 2021). This
138 substrate specificity has been observed in *in vitro* or cell-based studies (Gijón et al., 2008;

139 Zarini et al., 2014; Caddeo A., et al., 2019; Caddeo A., et al. 2021), which has been confirmed
140 *in vivo* in mice with diminished *Mboat7* function (Helsley et al., 2019; Meroni et al., 2020;
141 Tanaka et al., 2021; Thangapandi et al., 2021; Xia et al., 2021). Although MBOAT7 is well
142 documented to directly modulate PI lipids, the Land's cycle is highly dynamic and has the
143 potential to influence many downstream metabolic processes as well as cell signaling. Here we
144 report that ethanol-induced perturbation of the hepatic lipidome is powerfully shaped by
145 MBOAT7 function in hepatocytes. This MBOAT7-dependent reorganization of the hepatic
146 lipidome in response to ethanol is also functionally tied to diminished lysosome function and
147 defective autophagy. This work shows that MBOAT7 uniquely contributes to ethanol-induced
148 liver injury via perturbations of hepatic lipid metabolism that extend beyond the direct
149 remodeling of membrane PI.

150

151 **Results**

152

153 **Heavy drinkers have reduced circulating levels of MBOAT7 enzymatic products**

154 Given previous studies have shown that MBOAT7 is a risk locus for alcohol-associated
155 cirrhosis (Buchs et al., 2015), we investigated whether active alcohol consumption was
156 associated with alterations in MBOAT7 function. To address this, we measured both LPI
157 substrates and PI products of the MBOAT7 enzymatic reaction in the circulation of healthy
158 controls compared to confirmed heavy drinkers (**Figure 1**). Heavy drinkers were recruited and
159 defined by an AUDIT score (Fleming et al., 1991) greater than 16, and compared to an age-
160 and sex-matched healthy control population (**Figure 1 – figure supplement 1**). In agreement
161 with genetic studies linking MBOAT7 variants to alcohol-associated cirrhosis (Buchs et al.,
162 2015), we find that circulating levels of metabolic products of MBOAT7 including arachidonic

163 acid- and eicosapentaenoic acid-containing phophosphatidylinositols (PI 38:4 & PI 38:5) are
164 significantly reduced in heavy drinkers compared to age-matched healthy controls **(Figure 1)**.
165 Given MBOAT7 demonstrates specificity for polyunsaturated (PUFA) acyl-CoA substrates
166 (Gijón et al., 2008), it is important to note that only select PUFA-containing MBOAT7 products
167 (PI 38:4 and PI 38:5) were reduced in heavy drinkers, whereas all other molecular species of
168 PI were unaltered. We also examined the circulating levels LPI substrates of MBOAT7 but
169 found no significant differences between controls and heavy drinkers (**Figure 1**). These data
170 show that excessive alcoholic intake is associated with reduced levels of MBOAT7 product
171 lipids, which further bolsters the concept that MBOAT7 loss of function may be causally linked
172 to ALD progression.
173

174 **MBOAT7 loss of function in hepatocytes, but not myeloid cells, facilitates ethanol-**
175 **induced liver injury in mice**

176 Although there is some emerging evidence that MBOAT7 genetic variants may predispose
177 humans to alcohol-induced liver injury (Buchs et al., 2015), not all human studies have found a
178 significant association (Zhang et al., 2018; Stickel et al., 2018; Beaudoin et al., 2021).
179 Importantly, a causal relationship between MBOAT7 and alcohol-induced liver injury has never
180 been established to date. To address this, we have studied ethanol-induced liver injury in mice
181 selectively lacking *Mboat7* in hepatocytes or myeloid cells, given the key roles that
182 hepatocytes and myeloid cells play in the pathogenesis of ethanol-induced liver disease
183 progression. To generate congenic hepatocyte-specific (*Mboat7*^{HSKO}) and myeloid-specific
184 (*Mboat7*^{MSKO}) *Mboat7* knockout mice we crossed mice harboring a post-FLP recombinase
185 conditionally targeted *Mboat7* floxed allele (Anderson et al., 2013; Massey et al., 2023) to mice
186 transgenically expressing Cre recombinase under the albumin promoter/enhancer (Postic et
187 al., 1999) or Cre knocked into the M lysozyme locus (Clausen et al., 1999) respectively. These

188 independent *Mboat7*^{HSKO} and *Mboat7*^{MSKO} lines were then backcrossed mice > 10 generations
189 into the C57BL/6J background and subsequently subjected to ethanol exposure. Compared to
190 control mice (*Mboat7*$^{flox/flox}$), *Mboat7*^{HSKO} mice had significantly reduced *Mboat7* mRNA and
191 protein expression in the liver (**Figure 2a,2b**), but not in other tissues (data not shown; Massey
192 et al., 2023). Hepatocyte-specific deletion of *Mboat7* resulted in enhanced ethanol-induced
193 increases in liver weight and high concentrations of plasma alanine aminotransferase (ALT)
194 (**Figure 2c,2d**). Likewise, *Mboat7*^{HSKO} mice showed elevated hepatic steatosis scores and
195 triglyceride levels under both pair-fed and ethanol-fed conditions (**Figure 2e,2f**). However,
196 hepatocyte-specific deletion of *Mboat7* did not significantly alter the mRNA expression for
197 several proinflammatory cytokines/chemokines including tumor necrosis factor α (*Tnfα*),
198 transforming growth factor β (*Tgfβ*), monocyte chemoattractant protein 1 (*Mcp1*), or
199 interleukins 1β (*IL-1β*) or 6 (*IL-6*) in either pair-fed or ethanol-fed conditions (**Figure 2g**). These
200 data demonstrate that MBOAT7 function in hepatocytes is a critical determinant of ethanol-
201 induced liver injury, but we also wanted to explore a potential role for MBOAT7 in non-
202 parenchymal cells given the key roles that macrophages and neutrophils play in ALD.

203 It is important to note during the preparation of this manuscript, an independent study
204 discovered a potential role for MBOAT7 in suppressing toll-like receptor (TLR) signaling and
205 pro-inflammatory cytokine production in macrophages and Kupffer cells in the context of non-
206 alcoholic fatty liver disease (NAFLD) (Alharthi et al., 2022). Furthermore, early studies
207 examining the expression and substrate specificity for diverse lysophospholipid
208 acyltransferases showed that MBOAT7-driven PI remodeling was highly active in human
209 neutrophils where it can modulate the production of pro-inflammatory arachidonic acid-derived
210 lipid mediators (Gijón et al., 2008). Therefore, we generated myeloid-specific (*Mboat7*^{MSKO})
211 *Mboat7* knockout mice to further interrogate cell autonomous roles in ALD progression. First to
212 confirm efficient deletion in myeloid cells, we isolated both bone marrow-derived and

213 thioglycolate-elicited macrophages from control and myeloid-specific (*Mboat7*^{MSKO}) *Mboat7*
214 knockout mice, which confirmed essentially no detectable MBOAT7 protein in *Mboat7*^{MSKO}
215 mice (**Figure 2 – figure supplement 1**). In contrast to the enhanced ethanol-induced liver
216 injury seen in *Mboat7*^{HSKO} mice (**Figure 2**), myeloid-specific (*Mboat7*^{MSKO}) *Mboat7* deletion
217 resulted in unaltered ethanol-induced effects on body weight, liver weight, circulating levels of
218 aspartate and alanine aminotransferases (AST and ALT), liver triglyceride, and cytokine
219 expression (**Figure 2 – figure supplement 1**). Collectively, these results demonstrate that
220 MBOAT7 loss of function in hepatocytes, but not myeloid cells, facilitates ethanol-induced liver
221 injury in mice.
222

223 **Ethanol exposure reorganizes the hepatic lipidome in a MBOAT7-dependent manner**

224 Given the fact that ethanol exposure is well known to reorganize hepatic lipid metabolism, we
225 performed comprehensive lipidomic profiling of the liver to understand how MBOAT7 could
226 potentially shape ethanol-induced lipid metabolism in the liver. First, we used a targeted
227 approach to measure the levels of MBOAT7 substrate LPIs and product PIs. Compared to
228 control mice (*Mboat7*$^{flox/flox}$), *Mboat7*^{HSKO} mice had significant accumulation of palmitate- and
229 oleate-containing LPI substrate lipids (LPI 16:0 and LPI 18:1), with large accumulation of LPI
230 16:0 under ethanol-fed conditions (**Figure 3a**). When we examined PI species, we confirmed
231 previous findings that *Mboat7*^{HSKO} mice have reduced levels of the major arachidonic acid-
232 containing PI (PI 38:4) and also striking reductions in PI 38:3 under both pair- and ethanol-fed
233 conditions (**Figure 3b**). In addition, *Mboat7*^{HSKO} mice also have accumulation of several other
234 PI species including PI 34:1, PI 36:1, PI 36:2, PI 38:6, and PI 40:6, some of which are
235 exacerbated in the ethanol-fed group (**Figure 3c**). Although many of these changes in
236 MBOAT7's substrate LPIs and product PIs are expected based on MBOAT7's substrate
237 specificity and previous literature, there is a clear interaction between ethanol and MBOAT7

238 uncovered here that has not been observed in studies using NAFLD-related models (Tanaka
239 et al., 2021; Thangapandi et al., 2021; Xia et al., 2021).

240 Given this unexpected interaction between ethanol exposure and MBOAT7 within the
241 inositol-containing phospholipid pool, we examined the hepatic lipidome more broadly. Using
242 untargeted lipidomics, we identified a striking remodeling of the global hepatic lipidome upon
243 ethanol feeding in *Mboat7*^{HSKO} mice (**Figure 3 & Figure 3 – figure supplements 1-11**).
244 Unexpectedly, we observed a large increase in the levels of endosomal/lysosomal lipids
245 including bis(monoacylglycero)phosphates (BMPs) and their outer mitochondrial membrane
246 precursor phosphatidylglycerols (PGs) in ethanol-exposed *Mboat7*^{HSKO} mice (**Figure 3e-3g;**
247 **Figure 3 – figure supplement 3 & 4**). In addition, *Mboat7*^{HSKO} mice had elevated levels of
248 cardiolipin species, which are known to localize to mitochondria (**Figure 3e,3h; Figure 3 –**
249 **figure supplement 5**). Under the pair- and ethanol-fed conditions studies here, *Mboat7*^{HSKO}
250 mice also exhibited some more minor alterations in certain species of phosphatidylcholine
251 (PC), phosphatidylethanolamine (PE), phosphatidylserine (PS), phosphatidic acid (PA),
252 sphingomyelin (SM), ceramides (Cer), and ether-linked phospholipids (**Figure 3e; Figure 3 –**
253 **figure supplements 2, 7, 6, 8, 9, 10,11**). Although several recent studies examining
254 hepatocyte-specific *Mboat7*^{HSKO} mice have found more limited effects on the global lipidome
255 under experimental conditions designed to stimulate non-alcoholic steatohepatitis (NASH)
256 (Tanaka et al., 2021; Thangapandi et al., 2021; Xia et al., 2021), here we show that upon
257 ethanol exposure, hepatocyte MBOAT7 plays a major role in shaping endosomal/lysosomal
258 lipid homeostasis.

259

260 ***Mboat7*^{HSKO} mice have dysregulated lysosomal function in response to ethanol**

261 Given the accumulation of endosomal/lysosomal lipids including BMPs seen in ethanol-fed
262 *Mboat7*^{HSKO} mice, we hypothesized that ethanol may perturb lysosome function in a MBOAT7-

263 driven manner to promote liver injury. It is well known that BMPs commonly accumulate in both
264 drug-induced and genetic lysosomal storage disorders (Gruenberg 2020; Showalter et al.,
265 2020; Hullin-Matsuda et al., 2014), and due to their cone-shaped structure BMPs can
266 contribute to significant membrane asymmetry that impacts intracellular lipid sorting, apoptosis,
267 and autophagic flux (Gruenberg 2020; Showalter et al., 2020; Hullin-Matsuda et al., 2014). At
268 the same time, there is emerging evidence that chronic ethanol exposure can reduce the
269 expression of transcription factor EB (TFEB), which is a master regulator of lysosomal
270 biogenesis and autophagy-associated gene expression (Chao et al., 2018). Given the role that
271 lysosomal dysfunction plays in ethanol-induced liver injury (Chao et al., 2018; Bala and Szabo
272 2018), and the unexpected accumulation of BMP lipids in *Mboat7*^{HSKO} mice, we next
273 investigated TFEB-mediated lysosomal biogenesis and autophagy regulation in *Mboat7*^{HSKO}
274 mice challenged with ethanol (**Figure 4**). First, *Mboat7*^{HSKO} mice showed elevated levels of key
275 autophagy regulatory proteins LC3-I/II and p62 in the liver, particularly under ethanol-fed
276 conditions (**Figure 4a**). Interestingly, *Mboat7*^{HSKO} mice also had increased total levels of the
277 mammalian target of rapamycin (mTOR) (**Figure 4a**), which is a well-known master regulator
278 of autophagic flux. The accumulation of p62 and LC3-I/II cannot distinguish between enhanced
279 or defective autophagic flux, so we next examined potential alterations in lysosome abundance
280 and function. Interestingly, both mRNA and protein levels of lysosomal marker proteins LAMP-
281 1 and LAMP-2 were reduced in ethanol-fed *Mboat7*^{HSKO} mice (**Figure 4a,4d**). Furthermore,
282 compared to control mice fed ethanol, we found that ethanol *Mboat7*^{HSKO} mice had generally
283 reduced expressions levels of TFEB target genes and proteins associated with lysosome
284 acidification and lipid turnover including ATPase H+ transporting V1 subunits A,H, and D
285 (*Atp6v1a, Atp6v1h, Atp6v1d*), α galactosidase A (*Gla*), chloride channel 7 α (*Clcn7*), and
286 mucolipin TRP cation channel 1 (*Mcoln1*) (**Figure 4a,4d**). Similarly, the mRNA expression, and
287 total and nuclear protein abundance of TFEB was reduced in ethanol-fed *Mboat7*^{HSKO} mice

288 compared to ethanol-fed *Mboat7*$^{flox/flox}$ control mice (**Figure 4a,4b,4d**). In contrast, the
289 expression of key autophagy related genes including *Atg2b, Atg3, Atg7, Atg8/LC3*, and Unc-
290 51-like autophagy activating kinase 1 (*Ulk1*) were significantly elevated in ethanol-fed
291 *Mboat7*^{HSKO} mice compared to ethanol-fed *Mboat7*$^{flox/flox}$ control mice (**Figure 4d**).

292 We next investigated the cell autonomous effects of ethanol on wild type human Huh7
293 hepatoma cells or Huh7 cells genetically lacking *MBOAT7* (*MBOAT7*Δ-Huh7). In agreement
294 with what we found in mouse liver, *MBOAT7*Δ-Huh7 cells had reduced levels of total TFEB and
295 lysosomal marker proteins including LAMP1-, LAMP-2, and ATP6V1A, (**Figure 4 – figure**
296 **supplement 1**). Furthermore, *MBOAT7*Δ-Huh7 cells had increased levels of LC3 and total
297 mTOR, which was particularly apparent upon ethanol exposure (**Figure 4 – figure**
298 **supplement 1**). We next assessed lysosome protein degradation activity in wild type and
299 MBOAT7Δ-Huh7 hepatoma cells by measuring the degradation of an exogenous lysosome
300 indicator, quantified via median Bodipy/Alexa647 fluorescence ratio. In the absence of ethanol
301 treatment, there was no significant difference in the lysosomal activity between wild type and
302 MBOAT7Δ-Huh7 cells. Lysosome activity was increased by 42% in wild type cells with ethanol
303 treatment vs. no treatment ($p<0.001$. **Figure 4c**), in agreement with increased mRNA levels of
304 several lysosomal hydrolases (**Figure 4d**). However, the lysosome activity was decreased by
305 45% in MBOAT7Δ-Huh7 vs. wild type cells treated with ethanol ($p<0.001$, **Figure 4c**).
306 Collectively, in the presence of EtOH, deletion of *MBOAT7* in mouse or human hepatocytes
307 results in defective TFEB-mediated lysosomal biogenesis and lysosome activity, which would
308 be expected to lead to impaired autophagic flux.

309

310 **Discussion**

311 This manuscript builds on our initial observation that ASO-mediated knockdown of *Mboat7*

312 promotes NAFLD progression, hyperinsulinemia, and insulin resistance in mice (Helsley et al.,
313 2019). Here we have further clarified the cell autonomous roles of *Mboat7* in ethanol-driven
314 liver injury by comparing metabolic phenotypes in hepatocyte-specific (*Mboat7*^{HSKO}) and
315 myeloid-specific (*Mboat7*^{MSKO}) mice. The major findings of the current study include the
316 following: (1) MBOAT7 product PI species (PI 38:4 and PI 38:5) are reduced in the circulation
317 of human consuming high levels of alcohol, (2) MBOAT7 loss of function in hepatocytes, but
318 not myeloid cells, promotes ethanol-induced liver injury in mice, (3) Hepatocyte-specific
319 deletion of *Mboat7* results in expected alterations in substrate LPI and product PI lipids, but
320 unexpectedly alters lysosomal/endosome BMP lipids in an ethanol-driven manner, (4) Genetic
321 deletion in mouse or human hepatocytes results in dysregulation of lysosomal biogenesis and
322 autophagic flux, particularly under ethanol-challenged conditions. This works provides new
323 insights into how genetic variation in *MBOAT7* may impact ALD progression in humans and
324 mice. Importantly, this work is the first to causally link MBOAT7 loss of function in hepatocytes,
325 but not myeloid cells, to ethanol-induced liver injury via dysregulation of lysosomal biogenesis
326 and autophagic flux. Although not all human studies agree there is a uniform association
327 between the rs641738 SNP with alcohol-associated liver disease, our work indicate a very
328 powerful interaction between MBOAT7 loss of function and ethanol-induced liver injury.

329 Here we have identified a striking reorganization of the hepatic lipidome in *Mboat7*^{HSKO} mice
330 when exposed to ethanol (**Figure 3; Figure 3 – figure supplements 1-11**). In previous
331 independent studies examining lipid alterations in *Mboat7*^{HSKO} mice under experimental
332 conditions to elicit NAFLD and fibrosis (i.e. high fat diets or methionine/choline-deficient diets),
333 the global lipidomic alterations in the liver were much more confined to inositol-containing
334 phospholipids and triacylglycerols (Tanaka et al., 2019; Thangapandi et al., 2019). It is
335 important to note that the work of Xia and colleagues did previously report increased levels on
336 PG lipids specifically in isolated endoplasmic reticulum (ER) membranes from *Mboat7*^{HSKO}

337 mice, but our work confirms and extends this to show that not only PG but precursor BMPs are
338 significantly elevated in *Mboat7*^{HSKO} mice, particularly when challenged with ethanol. It is still
339 unclear how MBOAT7 impacts endosomal/lysosomal BMP and mitochondrial lipids such as
340 PG and CL under ethanol-exposed conditions, but our work clearly indicates that ethanol
341 reorganizes the global liver lipidome in a MBOAT7-dependent manner. It is most likely that the
342 accumulation of BMP and PG lipids seen in ethanol-challenged *Mboat7*^{HSKO} mice are not
343 directly related to the lysophospholipid acyltransferase activity of MBOAT7. Instead, it is more
344 plausible that the accumulation of BMPs and PGs seen in *Mboat7*^{HSKO} mice is secondary to
345 indirect reorganization of the arachidonate PI cycle or other related lipid metabolic pathways
346 coordinated at the ER.

347 For instance, the arachidonate PI cycle is initiated in the ER where inositol is added to
348 CDP-diacylglycerol (18:0/20:4) by phosphatidylinositol synthase (PIS) to produce the exact
349 same metabolic product of MBOAT7 (PI 38:4). It is likely that both PIS-generated as well as
350 MBOAT7-generated PI 38:4 can serve as a substrate for phosphatidylinositol kinases to form
351 the key second messengers known as PI phosphates [PIPs including PI(18:0/20:4)-4P,
352 PI(18:0/20:4)-4,5P_2,] and related lipid mediators downstream of phospholipase C in the
353 arachidonate PI cycle [IP3, DAG(18:0/20:4), PA(18:0/20:4), and CDP-DAG(18:0/20:4). It is
354 important to note that seminal work by Anderson and colleagues (Anderson et al., 2013) found
355 that total PIPs, PI(18:0/20:4)-4P, and PI(18:0/20:4)-4,5P_2 were significantly reduced in global
356 *Mboat7*$^{-/-}$ mice. In fact, more than 85% of PIP species in cultured cells have an *sn*-1 18:0 and
357 *sn*-2 20:4 acyl chain composition (i.e., in part originate from the MBOAT7 and PIS product PI
358 38:4) (Clark et al., 2011; Rouzer et al., 2007). These reductions in PIPs seen with *Mboat7*
359 deficiency (Anderson et al., 2013) could have important consequences in cellular signal
360 transduction, given that PIPs are common second messengers generated downstream of
361 ligand activation of numerous receptor systems including hormone, growth factor, cytokine,

362 and chemokine receptors (Wymann and Schneiter 2008; Pemberton et al., 2020; Fruman et
363 al., 2017; Hoxhaj and Manning 2020). PIPs also play diverse roles in shaping protein-lipid
364 interactions, membrane fusion events, vesicular transport, solute channel function, and
365 cytoskeletal arrangement (Wymann and Schneiter 2008; Pemberton et al., 2020; Fruman et
366 al., 2017; Hoxhaj and Manning 2020). Most relevant to this work, anionic lipids play very
367 important roles in controlling membrane dynamics that shape nearly all steps of autophagy
368 including initiation of autophagosome biogenesis and autophagosome-lysosome fusion (Baba
369 and Balla 2020; Schink et al., 2016). Collectively, given the fact that MBOAT7 generates the
370 most abundant species of PI (PI 38:4), and key cellular PIPs [PI(18:0/20:4)-4P, and
371 PI(18:0/20:4)-4,5P_2] there is a strong potential that the primary alterations in PI and PIP lipids
372 could broadly alter cellular signal transduction, endosomal/lysosomal lipid sorting, membrane
373 fusion events, vesicular transport, solute channel function, cytoskeletal arrangement, and
374 autophagic flux.

375 Collectively, this works provides new cellular and molecular insights into how genetic
376 variation in *MBOAT7* impacts ALD progression in humans and mice. This work is the first to
377 causally link MBOAT7 loss of function in hepatocytes, but not myeloid cells, to ethanol-induced
378 liver injury via dysregulation of lysosomal biogenesis and autophagic flux and broaden our
379 understanding of the lipid metabolic mechanisms promoting ethanol-induced liver injury. This
380 work also shows that MBOAT7-driven LPI acylation in the ER can indirectly impact both
381 lysosomal (BMP) and mitochondrial (CL and PG) lipids which can have broad impacts on
382 autophagy described here, as well as defective fatty acid oxidation as we originally reported in
383 high fat diet-fed mice (Helsley et al., 2019). The results of this work have broad potential
384 implications in the management of both alcoholic- and non-alcoholic fatty liver disease,
385 indicating that strategies that effectively restore both lysosomal and mitochondrial function may
386 hold some therapeutic promise in humans with the common MBOAT7 rs641738 variant.

Key Resource Table					

387

388

389

390

391

392

393

394

395

396 **KEY RESOURCE TABLE:**

Reagent type (species) or resource	Designation	Source or Reference	Identifiers	Additional Information	Research Resource Identifiers (RRID)
Genetic reagent (*M.musculus*)	*Mboat7tm1a(KOMP)Wtsi/ Mboat7tm1a(KOMP)Wtsi*	PMID: 23472195			RRID:MGI:5510874
Genetic reagent (*M.musculus*)	*B6N.Cg-Speer6-ps1*$^{Tg(Alb-cre)21Mgn}$*/J*	Jackson Laboratory	Stock#: 018961		RRID:IMSR_JAX:018961
Genetic reagent (*M.musculus*)	*B6.129P2-Lyz2*$^{tm1(cre)Ifo}$*/J*	Jackson Laboratory	Stock#: 004781		RRID:IMSR_JAX:004781
Antibody	Anti-MBOAT7 (Rat monoclonal)	PMID: 23097495		1:1000	RRID: AB_2813851
Antibody	Anti-Rat-HRP	Cell Signaling	Cat#: 7077	1:5000	RRID: AB_10694715
Antibody	LC3A/B (D3U4C) XP® Rabbit mAb	Cell Signaling	Cat#: 12741	1:1000	RRID: AB_2617131
Antibody	SQSTM1/p62 Antibody	Cell Signaling	Cat#: 5114	1:1000	RRID: AB_10624872
Antibody	mTOR (7C10) Rabbit mAb	Cell Signaling	Cat#: 2983	1:1000	RRID: AB_2105622
Antibody	TFEB Rabbit mAb 37785	Cell Signaling	Cat#: D207D	1:1000	
Antibody	LAMP1 (D2D11) XP® Rabbit mAb	Cell Signaling	Cat#: 9091	1:1000	
Antibody	LAMP2 (D5C2P) Rabbit mAb #49067	Cell Signaling	Cat#: 49067	1:1000	RRID: AB_2799349
Antibody	ATP6V1A polyclonal antibody	GeneTex	Cat#: GTX110815	1:1000	
Antibody	Anti-GAPDH-HRP (Rabbit monoclonal)	Cell Signaling	Cat#: 8884	1:5000	RRID: AB_11129865
Antibody	Lamin A/C (4C11) Mouse mAb	Cell Signaling	Cat#: 4777	1:1000	RRID:
Antibody	HRP-conjugated Beta Actin Monoclonal antibody	Proteintech	Cat#: HRP-60008	1:10000	RRID: AB_2289225
Commercial assay kit	ALT kit	Sekisui Diagnostics	318-30		
Commercial assay kit	AST kit	Sekisui Diagnostics	319-30		
Commercial assay kit	Liver TG	Wako	994-02891		
Commercial assay kit	Microsome Isolation	Abcam	ab206995		
Commercial assay kit	NE-PER™ Nuclear and Cytoplasmic Extraction Reagents	ThermoFisher Scientific	78833		
Commercial assay kit	Supersignal West Pico Plus substrate	ThermoFisher Scientific	34577		
Chemical or Solvent	Ammonium formate	Honeywell	Cat# 55674		
Chemical or Solvent	Methanol	Honeywell	Cat# LC230-4		
Chemical or Solvent	Water	Honeywell	Cat# LC365-4		
Chemical or Solvent	Acetonitrile	Honeywell	Cat# LC015-4		
Chemical or Solvent	Isopropanol	Fisher Scientific	Cat# A461-4		
Chemical or Solvent	Ethyl acetate	Sigma-Aldrich	Cat# 650528		

Chemical or Solvent	Formic acid	Thermo Scientific	Cat# 28905		
Chemical Compound	FA $18:0_{d35}$	Cayman Chemical	Cat# 9003318		
Chemical Compound	ACar $18:1_{d3}$	Cayman Chemical	Cat# 26578		
Chemical Compound	BMP 14:0_14:0	Avanti	Cat# 857131		
Chemical Compound	PG 15:0_$18:1_{d7}$	Avanti	Cat# 91640		
Chemical Compound	Cer $d18:1_{d7}$_15:0	Avanti	Cat# 860681P		
Chemical Compound	PA 15:0_$18:1_{d7}$	Avanti	Cat# 791642		
Chemical Compound	SPLASH LipidoMix II	Avanti	Cat# 330709		
Chemical Compound	BMP 18:1_18:1	Avanti	Cat# 857133P		
Chemical Compound	PG 18:1_18:1	Avanti	Cat# 840475P		
Sequence Based Reagent	Mboat7 Fwd	Sigma	5'-CATGCGGTACTGGAACATGA-3'		
Sequence Based Reagent	Mboat7 Rev	Sigma	5'-CCAGTAGGCGCTCAGCAG-3'		
Sequence Based Reagent	Cyclophilin A Fwd	Sigma	5'-GCGGCAGGTCCATCTACG-3'		
Sequence Based Reagent	Cyclophilin A Rev	Sigma	5'-GCCATCCAGCCATTCAGTC-3'		
Sequence Based Reagent	Tnfalpha Fwd	Sigma	5'-CCACCACGCTCTTCTGTCTAC -3'		
Sequence Based Reagent	Tnfalpha Rev	Sigma	5'-AGGGTCTGGGCCATAGAACT-3'		
Sequence Based Reagent	IL-1β Fwd	Sigma	5'-AGTTGACGGACCCCAAAAG -3'		
Sequence Based Reagent	IL-1β Rev	Sigma	5'-AGCTGGATGCTCTCATCAGG -3'		
Sequence Based Reagent	Tgf β Fwd	Sigma	5'-TGGAGCAACATGTGGAACTC-3'		
Sequence Based Reagent	Tgf βRev	Sigma	5'-CAGCAGCCGGTTACCAAG-3'		
Sequence Based Reagent	IL-6 Fwd	Sigma	5'-GCTACCAAACTGGATATAATCAGGA-3'		
Sequence Based Reagent	IL-6 Rev	Sigma	5'-CCAGGTAGCTATGGTACTCCAGAA-3'		
Sequence Based Reagent	Mcp-1 Fwd	Sigma	5'-TTCCTCCACCACCATGCAG-3'		
Sequence Based Reagent	Mcp-1 Rev	Sigma	5'-CCAGCCGGCAACTGTGA-3'		

Sequence Based Reagent	TFEB Fwd	Sigma	5'-CCAGAAGCGAGAGCTCACAGAT-3'		
Sequence Based Reagent	TFEB Rev	Sigma	5'-TGTGATTGTCTTTCTTCTGCCG-3'		
Sequence Based Reagent	Lamp-1 Fwd	Sigma	5'-AGCATACCGGTGTGTCAGTG-3'		
Sequence Based Reagent	Lamp-1 Rev	Sigma	5'-GTTGGGGAAGGTCCATCCTG-3'		
Sequence Based Reagent	Lamp-2 Fwd	Sigma	5'-TGCAGTGCAGATGAAGACAAC-3'		
Sequence Based Reagent	Lamp-2 Rev	Sigma	5'-GCTATGGGCACAAGGAAGTTG-3'		
Sequence Based Reagent	Ctsa Fwd	Sigma	5'-GCTACCTCAGAGCATCGGAC-3'		
Sequence Based Reagent	Ctsa Rev	Sigma	5'-GTTAAGCCAAAGCACCACGG-3'		
Sequence Based Reagent	Gba Fwd	Sigma	5'-GCCTCCCAGAAGAAGACACC-3'		
Sequence Based Reagent	Gba Rev	Sigma	5'-ATATCCCCTGGCTGACCCTT-3'		
Sequence Based Reagent	Gla Fwd	Sigma	5'-TTGGGGTCAGAGCA TTGGAC-3'		
Sequence Based Reagent	Gla Rev	Sigma	5'-AGTCATAACCTGCATCCCGC-3'		
Sequence Based Reagent	Psap Fwd	Sigma	5'-CAGCAGATGGTCTGGAGCAA-3'		
Sequence Based Reagent	Psap Rev	Sigma	5'-CAAGTTCCCAGCTTCGGTGA-3'		
Sequence Based Reagent	Clcn7 Fwd	Sigma	5'-CGAGATGCCTATCCACGCTT-3'		
Sequence Based Reagent	Clcn7 Rev	Sigma	5'-CCCGGAAGAGCTTGAACACT-3'		
Sequence Based Reagent	Mcoln1 Fwd	Sigma	5'-TGGGCCAATGGATCAGCTTT-3'		
Sequence Based Reagent	Mcoln1 Rev	Sigma	5'-GTTCTTGTAACTGGCGCTGC-3'		

Sequence Based Reagent	Atp6v1h Fwd	Sigma	5'-AAGACCAGCAGGTTCGCTAC-3'		
Sequence Based Reagent	Atp6v1h Rev	Sigma	5'-TGCAGAAAGGCTGAACAGGT-3'		
Sequence Based Reagent	Atp6v1d Fwd	Sigma	5'-GAGCACAGACTGGTCGAAA-3'		
Sequence Based Reagent	Atp6v1d Rev	Sigma	5'-AGCTGTCAGTTCCTTCGTGG-3'		
Sequence Based Reagent	ULK1 Fwd	Sigma	5'-ACCATTGTCTACCAGTGT-3'		
Sequence Based Reagent	ULK1 Rev	Sigma	5'-AGTGTCTTGTTCTTCTCATAA-3'		
Sequence Based Reagent	Atg2b Fwd	Sigma	5'-CCTCCACTCTCAGAATCA-3'		
Sequence Based Reagent	Atg2b Rev	Sigma	5'-GTCCATCACACGAACATAA-3'		
Sequence Based Reagent	Atg3 Fwd	Sigma	5'-TCACAACACAGGTATTACAG-3'		
Sequence Based Reagent	Atg3 Rev	Sigma	5'-CTTCCTCGTCTTCTTCATC-3'		
Sequence Based Reagent	Atg7 Fwd	Sigma	5'-CAGAAGAAGTTGAACGAGTA-3'		
Sequence Based Reagent	Atg7 Rev	Sigma	5'-CAGAGTCACCATTGTAGTAAT-3'		
Sequence Based Reagent	Lc3 Fwd	Sigma	5'-GCTCTTTGTTGGTGTGTA-3'		
Sequence Based Reagent	Lc3 Rev	Sigma	5'-TCTTCTGTTGCTGTTGTC-3'		

397

398

399

400

401 **METHODS**

402 **Human studies**

403 *Healthy Control and Heavy Drinking Patient Selection* - Healthy controls or heavy drinkers with
404 an AUDIT score greater than >16 were recruited from the Clinical Research Unit at the
405 Cleveland Clinic or MetroHealth Hospital in Cleveland, Ohio based on medical history and
406 physical examination. The study protocol was approved by the Institutional review board for
407 the Protection of Human Subjects in Research at the Cleveland Clinic (IRB 17-718) and
408 MetroHealth Hospital Cleveland (IRB 18-00911). All methods were performed in accordance
409 with the internal review board's guidelines and regulations, and written, informed consent was
410 obtained from all subjects. Subject demographics are shown in Figure 1 – figure supplement 1.
411

412 **Mice and experimental diets**

413 To generate conditional *Mboat7* knockout mice, we obtained "knockout first"
414 (Mboat7$^{tm1a(KOMP)Wtsi}$) mice from Dr. Philip Hawkins (Anderson et al., 2013), and crossed these
415 mice with mice transgenically expressing FLP recombinase to remove the NEO cassette
416 resulting in a conditional *Mboat7* floxed allele. The FLP transgene was then subsequently bred
417 out of the line and resulting *Mboat7*$^{flox/WT}$ mice, which were used to expand further downstream
418 tissue-specific knockout lines. To generate congenic hepatocyte-specific (*Mboat7*^{HSKO}) and
419 myeloid-specific (*Mboat7*^{MSKO}) *Mboat7* knockout mice we crossed mice harboring a post-FLP
420 recombinase conditionally-targeted *Mboat7* floxed allele (Anderson et al., 2013; Massey et al.,
421 2023) to mice transgenically expressing Cre recombinase under the albumin
422 promoter/enhancer (Postic et al., 1999) or Cre knocked into the M lysozyme locus (Clausen et
423 al., 1999) respectively. These independent *Mboat7*^{HSKO} and *Mboat7*^{MSKO} lines were then
424 backcrossed mice > 10 generations into the C57BL/6J background and subsequently
425 subjected to ethanol exposure. Confirmation of sufficient backcrossing into the C57BL/6J
426 background was confirmed by mouse genome single nucleotide polymorphism (SNP) scanning
427 at the Jackson Laboratory (Bar Harbor, ME). Age- and weight-matched female (8-10 weeks

428 old) control (Mboat7$^{flox/flox}$), hepatocyte-specific *Mboat7* knockout mice (Mboat7^{HSKO}), or
429 myeloid-specific *Mboat7* knockout mice (Mboat7^{MSKO}) were maintained on a chow diet and
430 randomized into pair- and ethanol-fed groups using the NIAAA model (Bertola et al., 2013).
431 Briefly, mice were initially fed with control Lieber-DeCarli diet ad libitum for 5 days to
432 acclimatize them to liquid diet. Afterward, ethanol (EtOH)-fed groups were allowed free access
433 to the ethanol Lieber-DeCarli diet containing 5% (vol/vol) ethanol for 10 days, and control
434 groups were pair-fed with the isocaloric substituted maltose dextrins as control diet. At day 11,
435 ethanol-fed and pair-fed mice were gavaged in the early morning with a single dose of ethanol
436 (5 g/kg body weight) or isocaloric maltose dextrin, respectively, and euthanized 6 hours later.
437 (Bertola et al., 2013). All mice were maintained in an Association for the Assessment and
438 Accreditation of Laboratory Animal Care, International-approved animal facility, and all
439 experimental protocols were approved by the Institutional Animal Care and Use Committee of
440 the Cleveland Clinic (IACUC protocols # 2018-2053 and # 00002499).
441
442 **Histological analysis and imaging**
443 Hematoxylin and eosin (H&E) staining of paraffin-embedded liver sections was performed as
444 previously described (Gromovsky et al., 2017; Warrier et al., 2015; Brown et al., 2010; Brown
445 et al., 2008a; Brown et al. 2008b). Histopathologic evaluation was scored in a blinded fashion
446 by a board-certified pathologist with expertise in gastrointestinal/liver pathology (Daniela S.
447 Allende – Cleveland Clinic). H&E slides were scanned using a Leica Aperio AT2 Slide Scanner
448 (Leica Microsystems, GmbH, Wetzlar, Germany) and images were processed using
449 ImageScope (Aperio, Software Version 12.1
450
451 **Immunoblotting**

452 Whole tissue homogenates were made from tissues in a modified RIPA buffer as previously
453 described (Warrier et al., 2015; Helsley et al., 2019; Schugar et al., 2017; Lord et al., 2016),
454 microsome were isolated from the livers of control (*Mboat7*$^{fl/fl}$) or hepatocyte-specific *Mboat7*
455 knockout mice (*Mboat7*^{HSKO}) using microsome isolation kit from Abcam and protein was
456 quantified using the bicinchoninic assay (Pierce). Proteins were separated by 4–12% SDS-
457 PAGE, transferred to polyvinylidene difluoride membranes, and then proteins were detected
458 after incubation with specific antibodies as previously described (Warrier et al., 2015; Helsley
459 et al., 2019; Schugar et al., 2017; Lord et al., 2016) and listed in the Key resources table.
460

461 **Real-time PCR analysis of gene expression**

462 Tissue RNA extraction and qPCR analysis was performed as previously described (Helsley et
463 al., 2019). The mRNA expression levels were calculated based on the ΔΔ-CT method using
464 cyclophilin A as the housekeeping gene. qPCR was conducted using the Applied Biosystems
465 7500 Real-Time PCRsystem. All primer sequences are listed in the Key resources table.
466

467 **Plasma and liver biochemistries**

468 To determine the level of hepatic injury in mice fed HFD, plasma was used to analyze alanine
469 aminotransferase (ALT) levels using enzymatic assays as previously described (Helsley et al.,
470 2019). Extraction of liver lipids and quantification of total plasma and hepatic triglycerides was
471 conducted using enzymatic assays as described previously (Helsley et al., 2019; Gromovsky
472 et al., 2017).
473

474 **Liver lipid extraction**

475 Lipids were extracted from liver samples as previously described (Jain et al., 2022). Samples
476 were kept on ice throughout the extraction. Briefly, liver was homogenized in 500uL of 3:1:6

477 isopropanol:water:ethyl acetate containing internal standard in ceramic bead tubes (Qiagen
478 #13113-50) using the TissueLyzer II (Qiagen #9244420). Samples were centrifuged at
479 16,000xg for 10min at 4°C and the lipid containing supernatant was transferred to a new 1.5mL
480 tube. Lipid extracts were dried in a SpeedVac (Thermo Savant RVT5105) and resuspended in
481 150uL of methanol. Samples were kept at 4°C for no more than one week before analysis.
482

483 **Targeted quantification of lysophosphatidylinositol (LPI) and phosphatidylinositol (PI)**
484 **lipids**

485 Quantitation of LPI and PI species was performed as previously described (Helsley et al.,
486 2019) Briefly, LPI and PI standards (LPI 16:0, LPI 18:0, LPI 18:1, LPI 20:4, PI 38:4) and the
487 two internal standards (LPI 17:1-d31, PI 34:1-d31) were purchased Avanti Polar Lipids. HPLC
488 grade water, methanol and acetonitrile were purchased from Thermo Fisher Scientific.
489 Standard LPI and PI species at concentrations of 0, 5, 20, 100, 500 and 2000 ng/ml were
490 prepared in 90% methanol containing 2 internal standards at the concentration of 500 ng/ml.
491 Samples were injected into the Shimadzu LCMS-8050 for generating the internal standard
492 calibration curves. A triple quadrupole mass spectrometer (Quantiva, Thermos Fisher
493 Scientific, Waltham, MA, USA) was used for analysis of LPI and PI species. The mass
494 spectrometer was coupled to the outlet of an UHPLC system (Vanquish, Thermos Fisher
495 Scientific, Waltham, MA, USA), including an auto sampler with refrigerated sample
496 compartment and inline vacuum degasser. The HPLC eluent was directly injected into the
497 triple quadrupole mass spectrometer and the analytes were ionized at ESI negative mode.
498 Analytes were quantified using Selected Reaction Monitoring (SRM) and the SRM transitions
499 (m/z) were 571 → 255 for LPI 16:0, 599 → 283 for LPI 18:0, 597 → 281 for LPI 18:1, 619 →
500 303 for LPI 20:4, 885 → 241 for PI 38:4, 583 → 267 for internal standard LPI 17:1, and 866 →
501 281 for internal standard PI 34:1-d31. Xcalibur software was used to get the peak area for both

502 the internal standards and LPI and PI species. The internal standard calibration curves were
503 used to calculate the concentration of LPI and PI species in the samples.
504
505 **Untargeted Lipidomics**
506 Untargeted lipidomics was performed using an Agilent 1290 Infinity II liquid chromatograph
507 equipped with a Waters Acquity BEH C18 column (1.7 µm 2.1 × 100 mm) coupled to an
508 Agilent 6546 Q-TOF mass spectrometer. Mobile phase A was 60:40 acetonitrile:water and B
509 was 90:9:1 isopropanol:acetonitrile:water with both phases buffered with 10mM ammonium
510 formate and 0.1% formic acid. The gradient was as follows: starting at 15% B to 30% B at 2.40
511 min, 48% at 3 min, 82% at 13.2 min, 99% at 13.8 min then held at 99% until 15.4 min before
512 equilibrating 15%, held until 20 min. Samples were analyzed in both positive and negative
513 ionization in separate experiments with the following MS parameters: drying gas flowing 12
514 L/min at 250°C, nebulizer at 30 psi and sheath gas flowing 11 L/min at 300°C for positive
515 mode. The sheath gas flow was 12 L/min at 375°C with a nebulizer pressure of 30 psi in
516 negative mode. Both ionizations had the same voltage for capillary (4000 V), skimmer (75 V),
517 fragmentor (190 V) and octupole (750 V). Reference masses (m/z = 121.05 and 922 for
518 positive mode; 112.98 and 966.00 for negative mode) were continuously infused during
519 sample runs for accurate mass calibration. Pooled samples were run in consecutive iterative
520 MS/MS injections at a constant collision energy of 25V to collect spectra for lipid library
521 creation using Agilent LipidAnnotator and MS1 data was collected for all individual samples.
522 Peak integration was performed using Agilent Profinder (v8.0) software and further curation
523 and internal standard normalization was performed using in-house R scripts as described
524 previously (Jain et al., 2022). Untargeted data is reported in units of pmol lipid/g tissue.
525 Principal component analysis and heatmaps were generated using MetaboAnalyst (Pang et
526 al., 2021). The first and second principal components are plotted on the x- and y-axes,

527 respectively, and sample treatment group is indicated by color. For heatmap generation, data
528 was pareto-scaled and the normalized intensity is indicated by color with relative increase in
529 red and decrease in blue. The top 70 lipid features by ANOVA p-value are plotted on the y-axis
530 and samples are grouped by Ward clustering on the x-axis. Sample treatments are
531 distinguished by color.
532

533 **Targeted quantification of bis(monoacylglycerol)phosphates (BMPs) and**
534 **phosphatidylglycerols (PGs)**

535 Targeted BMP and PG lipid analysis was conducted on an Agilent 1290 Infinity II LC coupled
536 to an Agilent 6495C QQQ mass spectrometer. The same column, mobile phases, and gradient
537 were used for targeted analysis as for the untargeted. The MS parameters for both ionizations
538 were as follows: drying gas temp flow of 12 L/min at 250°C with nebulizer at 35 psi and sheath
539 gas flow of 11L/min at 300°C. Capillary voltage was kept at 4000 V with nozzle voltage of 500
540 V and collision energy = 20 V. The iFunnel high pressure RF was at 150/90 V and low-
541 pressure RF at 60/60 V for positive/negative ionizations, respectively. A sample type specific
542 lipid library was created by running pooled liver extract multiple times in positive ionization
543 using multiple reaction monitoring (MRM) to scan for a list of BMP/PG lipid precursor masses
544 ($[NH4]^{+}$ adducts) with transitions for the respective fatty acid and diacylglycerol (minus 17 m/z)
545 adducts (Grabner et al., 2020). BMPs were identified by the characteristic free fatty acid
546 fragment being much higher intensity than the diacylglycerol fragment, whereas the opposite
547 was true for PG. In addition, BMP lipids eluted between 0.3-0.5 min earlier than the isomeric
548 PG counterpart. These distinguishing characteristics were validated using commercial BMP
549 18:1_18:1 and PG 18:1_18:1 standards. A dynamic MRM method was created using the
550 retention time data gathered from positive ionization tests but in negative mode scanning for
551 the $[M-H]^{-}$ precursors and fatty acid fragments as BMP and PG are much more readily ionized

552 in negative mode. Data was integrated in Agilent Quantitative analysis and peaks were
553 manually adjusted and verified. Final units are in ng lipid/mg tissue.
554
555 **Lysosome protein degradation activity assay**
556 Lysosome protein degradation activity was performed as previously described (Robinet et al.,
557 2021). Briefly, DQ-ovalbumin (D12053, Thermofisher Scientific) was labeled with Alexa Fluor
558 647 succinimidyl ester (A20006, Thermofisher Scientific) at room temperature for 1 h (3:1
559 dye:protein mole ratio) to make lysosome protein degradation indicator. The reaction was
560 stopped by incubating the conjugate with 1.5 M hydroxylamine (pH 8.5) for 1h at room
561 temperature, and the conjugate was purified by extensive dialysis. Lysosome protein
562 degradation indicator was validated in vitro by incubating with proteinase K and achieving
563 significant increase of Bodipy/Alexa647 ratio (Robinet et al., 2021). The double labeled
564 ovalbumin has increased Bodipy fluorescence upon its degradation by decreasing its self-
565 quenching, while Alexa647 is not changed upon its degradation and is used to normalize for
566 cellular uptake. Wild type or MBOAT7Δ-Huh7 hepatoma cells treated with or without 100 mM
567 ethanol for 48 h were incubated with 10 µg/mL of lysosome indicator for 2 h, and lysosome
568 activity was analyzed by flow cytometry in ≈10,000 cells with a LSRFortessa device (BD).
569 Flowjo software was used to export data for each cell for ratiometric analyses, and the median
570 Bodipy/Alexa647 ratio for each independent well was used for analysis.
571
572 **Statistical analyses**
573 Single comparisons between two groups were performed using two-tailed Student's t tests with
574 95% confidence intervals. Comparisons involving multiple groups beyond binary comparison
575 were assessed using One-way ANOVA with Tukey's post-hoc test. All data presented as mean
576 ± SEM. Values were considered significant at $p < 0.05$ (using superscripts), or ***$p<0.001$ and

577 ****p<0.0001 in figure 1. JMP 17.0 statistical discovery software (SAS Institute, Cary, NC,
578 USA) was used for all statistical analyses.
579
580 **ACKNOWLEDGEMENTS**
581 This work was supported in part by National Institutes of Health grants P50 AA024333 (J.D.,
582 S.D., D.S.A., L.E.N., J.M.B.), R01 DK120679 (J.M.B.), RF1 NS133812 (J.M.B.), P01
583 HL147823 (J.M.B.), U01 AA026938 (L.E.N., J.M.B.), R01 DK130227 (J.M.B.), U01 AA026264
584 (L.E.N.), R01 HL128268 (J.D.S.), JDRF JDRF201309442 (J.S.), the Glenn and AFAR Junior
585 Faculty Grant A22068 (J.S.), R01 DK133479 (J.S.); Hatch Grant WIS04000 (R.J., J.S.), K01
586 DK128022 (R.N.H.), and UL1TR001998 (R.N.H.). The authors would like to thank Dr. Philip
587 Hawkins (Babraham Institute) for providing *Mboat7* knockout first mice.
588
589 **COMPETING FINANCIAL INTERESTS**
590 All other authors declare no competing financial interests related to this work.
591
592 **AUTHOR CONTRIBUTIONS**
593 V.V. and J.M.B. planned the project, designed experiments, and analyzed data. V.V. and
594 J.M.B. wrote the original draft of the manuscript; L.E.N., J.D.S., O.R., and J.S. helped design
595 experiments and provided useful discussion directing collaborative aspects of the project; V.V.,
596 I.R., W.J.M., R.J., R.B., A.J.H. 3rd, M.R.M., E.H., A.B., S.W.L., K.G., R.N.H., I.J., V.P., J.D.,
597 N.W., S.D., D.S., O.R., and D.S.A. either conducted mouse experiments, performed
598 biochemical workup of mouse tissues or analyzed data and aided in manuscript preparation.
599 All authors were involved in the editing of the final manuscript.
600
601

602 **DATA AVAILABILITY**

603 All materials, methods, and datasets included in this manuscript are readily available upon
604 request.

605

606 **LITERATURE CITED:**

607 Alharthi J, Bayoumi A, Thabet K, Pan Z, Gloss BS, Latchoumanin O, Lundberg M, Twine NA,
608 McLeod D, Alenizi S, Adams LA, Weltman M, Berg T, Liddle C, George J, Eslam M. 2022. A
609 metabolic associated fatty liver disease risk variant in MBOAT7 regulates toll like receptor
610 induced outcomes. *Nat. Commun.* **13:**7430.
611
612 Anderson KE, Kielkowska A, Durrant TN, Juvin V, Clark J, Stephens LR, Hawkins PT. 2013.
613 Lysophosphatidylinositol-acyltransferase-1 (LPIAT1) is required to maintain physiological
614 levels of PtdIns and PtdInsP(2) in the mouse. *PLoS One* **8:**e58425.
615
616 Baba, T., and T. Balla. 2020. Emerging roles of phosphatidylinositol 4-phosphate and
617 phosphatidylinositol 4,5-bisphosphate as regulators of multiple steps in autophagy. *J.*
618 *Biochem.* **168:**329-336.

619 Bala S, Szabo G. 2018. TFEB, a master regulator of lysosome biogenesis and autophagy, is a
620 new player in alcoholic liver disease. *Dig. Med. Res.* **1:**16.
621
622 Beaudoin JJ, Liang T, Tang Q, Banini BA, Shah VH, Sanyal AJ, Chalasani NP, Gawrieh S.
623 2021. Role of candidate gene variants in modulating the risk and severity of alcoholic hepatitis.
624 *Alcohol Clin. Exp. Res*. **45:**709-719.
625
626 Bertola A, Mathews S, Ki SH, Wang H, Gao B. 2013. Mouse model of chronic and binge
627 ethanol feeding (the NIAAA model). *Nat. Protoc.* **8**:627-637.
628
629 Buch S, Stickel F, Trepo E, Way M, Herrmann A, Nischalke HD, Brosch M, Rosendahl J, Berg
630 T, Ridinger M, Rietschel M, McQuillin A, Frank J, Kiefer F, Schreiber S, Lieb W, Soyka M,
631 Semmo N, Aigner E, Datz C, et al. 2015. A genome-wide association study confirms PNPLA3
632 and identifies TM6SF2 and MBOAT7 as risk loci for alcohol-related cirrhosis. *Nat. Genet.*
633 **47:**1443-1448.
634
635 Chao X, Wang S, Zhao K, Li Y, Williams JA, Li T, Chavan H, Krishnamurthy P, He XC, Li L,
636 Ballabio A, Ni HM, Ding WX. 2018. Impaired TFEB-mediated lysosome biogenesis and
637 autophagy promote chronic ethanol-induced liver injury and steatosis in mice.
638 *Gastroenterology* **155:**865-879.
639
640 Clausen BE, Burkhardt C, Reith W, Renkawitz R, Förster I. 1999. Conditional gene targeting in
641 macrophages and granulocytes using LysMcre mice. *Transgenic Res.* **8:**265-277.
642
643 Clark, J., K.E. Anderson, V. Juvin, T.S. Smith, F. Karpe, M.J. Wakelam, L.R. Stephens, and
644 P.T. Hawkins. 2011. Quantification of PtdInsP3 molecular species in cells and tissues by mass

645 spectrometry. *Nat. Methods* **8:**267-272.

646 Cohen JC, Horton JD, Hobbs, HH. 2011. Human fatty liver disease: old questions and new
647 insights. *Science* **332:**1519-1523.
648
649 Fleming MF, Barry KL, MacDonald R. 1991. The alcohol use disorders identification test
650 (AUDIT) in a college sample. *Int. J. Addict.* **26:**1173-1185.
651
652 Fruman, D.A., H. Chiu, B.D. Hopkins, S. Bagrodia, L.C. Cantley, and R.T. Abraham. 2017 The
653 PI3K pathway in human disease. *Cell* **170:**605-635.

654 Gijón MA., Riekhof WR, Zarini S, Murphy RC, Voelker DR. 2008. Lysophospholipid
655 acyltransferases and arachidonate recycling in human neutrophils. *J. Biol. Chem.* **283:**30235-
656 30245.
657
658 Grabner GF, Fawzy N, Pribasnig MA, Trieb M, Taschler U, Holzer M, Schweiger M, Wolinski
659 H, Kolb D, Horvath A, Breinbauer R, Rülicke T, Rabl R, Lass A, Stadlbauer V, Hutter-Paier B,
660 Stauber RE, Fickert P, Zechner R, Marsche G, Eichmann TO, Zimmermann R. 2019.
661 Metabolic disease and ABHD6 alter the circulating bis(monoacylglycerol)phosphate profile in
662 mice and humans. *J. Lipid Res.* **60:**1020-1031.
663
664 Gromovsky, A.D., Schugar RC, Brown AL, Helsley RN, Burrows AC, Ferguson D, Zhang R,
665 Sansbury BE, Lee RG, Morton RE, Allende DS, Parks JS, Spite M, Brown JM. 2017. Δ-5 Fatty
666 Acid Desaturase FADS1 Impacts Metabolic Disease by Balancing Proinflammatory and
667 Proresolving Lipid Mediators*.* Δ-5 fatty acid desaturase FADS1 impacts metabolic disease by
668 balancing proinflammatory and proresolving lipid mediators. *Arterioscler. Thromb. Vasc. Biol.*
669 **38:**218-231.
670
671 Gruenberg J. 2020. Life in the lumen: The multivesicular endosome. *Traffic* **21:**76-93.
672
673 Helsley RN, Varadharajan V, Brown AL, Gromovsky AD, Schugar RC, Ramachandiran I, Fung
674 K, Kabbany MN, Banerjee R, Neumann CK, Finney C, Pathak P, Orabi D, Osborn LJ, Massey
675 W, Zhang R, Kadam A, Sansbury BE, Pan C, Sacks J, et al. 2019. Obesity-linked suppression
676 of membrane-bound O-acyltransferase 7 (MBOAT7) drives non-alcoholic fatty liver disease.
677 *Elife* **8:**e49882.
678
679 Hoxhaj, G., and B.D. Manning. 2020. The PI3K-AKT network at the interface of oncogenic
680 signaling and cancer metabolism. *Nat. Rev. Cancer* **20:**74-88.

681 Hullin-Matsuda F, Taguchi T, Greimel P, Kobayashi T. 2014. Lipid compartmentalization in the
682 endosome system. *Semin. Cell. Dev. Biol.* **31:**48-56.
683
684 Jain R, Wade G, Ong I, Chaurasia B, Simcox J. 2022. Determination of tissue contributions to
685 the circulating lipid pool in cold exposure via systematic assessment of lipid profiles. *J. Lipid*
686 *Res*. **63:**100197.
687
688 Krawczyk, M., M. Rau, J. M. Schattenberg, H. Bantel, A. Pathil, M. Demir, J. Kluwe, T.
689 Boettler, F. Lammert, A. Geier, and N. C. S. Group. 2017. Combined effects of the PNPLA3
690 rs738409, TM6SF2 rs58542926, and MBOAT7 rs641738 variants on NAFLD severity: a
691 multicenter biopsy-based study. *J. Lipid Res.* **58:**247-255.

692
693 Mancina RM, Dongiovanni P, Petta S, Pingitore P, Meroni M, Rametta R, Boren J, Montalcini
694 T, Pujia A, Wiklund O, Hindy G, Spagnuolo R, Motta BM, Pipitone RM, Craxi A, Fargion S,
695 Nobili V, Kakela P, Karja V, Mannisto V, et al. 2016. The MBOAT7-TMC4 Variant rs641738
696 Increases Risk of Nonalcoholic Fatty Liver Disease in Individuals of European Descent.
697 *Gastroenterology* **150:**1219-1230.
698
699 Massey WJ, Varadharajan V, Banerjee R, Brown AL, Horak AJ, Hohe RC, Jung BM, Qiu Y,
700 Chan ER, Pan C, Zhang R, Allende DS, Willard B, Cheng F, Lusis AJ, Brown JM. 2023.
701 MBOAT7-driven lysophosphatidylinositol acylation in adipocytes contributes to systemic
702 glucose homeostasis. J*. Lipid Res.* **18:**100349.
703
704 Meroni MP. Dongiovanni M, Longo M, Carli F, Baselli G, Rametta R, Pelusi S, Badiali S,
705 Maggioni M, Gaggini M, Fracanzani AL, Romeo S, Gatti S, Davidson NO, Gastaldelli A, Valenti
706 L. 2020. Mboat7 down-regulation by hyper-insulinemia induces fat accumulation in
707 hepatocytes. *EBioMedicine* **52:**102658.
708
709 Pang Z, Chong J, Zhou G, de Lima Morais DA, Chang L, Barrette M, Gauthier C, Jacques PÉ,
710 Li S, Xia J. 2021. MetaboAnalyst 5.0: narrowing the gap between raw spectra and functional
711 insights. *Nucleic Acids Res*. **49(W1):**W388-W396.
712
713 Pemberton, J.G., Y.J. Kim, and T. Balla. 2020. Integrated regulation of phosphatidylinositol
714 cycle and phosphoinositide-driven lipid transport at ER-PM contact sites. *Traffic* **21:** 200-219.

715 Postic C, Shiota M, Niswender KD, Jetton TL, Chen Y, Moates JM, Shelton KD, Lindner J,
716 Cherrington AD, Magnuson MA. 1999. Dual roles for glucokinase in glucose homeostasis as
717 determined by liver and pancreatic beta cell-specific gene knock-outs using Cre recombinase.
718 *J. Biol. Chem.* **274:**305-315.
719
720 Rinella ME, Sanyal AJ. 2016. Management of NAFLD: a stage-based approach. *Nat. Rev.*
721 *Gastroenterol. Hepatol.* **13:**196-205.
722
723 Robinet P, Ritchey B, Lorkowski SW, Alzayed AM, DeGeorgia S, Schodowski E, Traughber
724 CA, Smith JD. 2021. Quantitative trait locus mapping identifies the Gpnmb gene as a modifier
725 of mouse macrophage lysosome function. Sci Rep. **11**:10249.
726
727 Rouzer, C.A., P.T. Ivanova, M.O. Byrne, H.A. Brown, and L.J. Marnett. 2007. Lipid profiling
728 reveals glycerophospholipid remodeling in zymosan-stimulated macrophages. *Biochemistry*
729 **46:**6026-6042.

730 Sabatine MS. 2019. PCSK9 inhibitors: clinical evidence and implementation. *Nat. Rev. Cardiol.*
731 16: 155-165.
732
733 Samuel VT, Shulman GI. 2018. Nonalcoholic fatty liver disease as a nexus of metabolic and
734 hepatic diseases. *Cell Metab.* **27:**22-41.
735
736 Schink, K.O., K.W. Tan, and H. Stenmark. 2016. Phosphoinositides in control of membrane
737 dynamics. *Annu. Rev. Cell. Dev. Biol*. **32:**143-171.

738 Schugar R, Shih DM, Warrier M, Helsley RN, Burrows A, Ferguson D, Brown AL, Gromovsky
739 AD, Heine M, Chatterjee A, Li L, Li XS, Wang Z, Willard B, Meng Y, Kim H, Che N, Pan C, Lee
740 RG, Crooke RM, Graham MJ, Morton RE, Langefeld CD, Das SK, Rudel LL, Zein N,
741 McCullough AJ, Dasarathy S, Tang WHW, Erokwu BO, Flask CA, Laakso M, Civelek M, Naga
742 Prasad SV, Heeren J, Lusis AJ, Hazen SL, Brown JM. 2017. The TMAO-producing enzyme
743 flavin-containing monooxygenase 3 regulates obesity and the beiging of white adipose tissue.
744 *Cell Rep.* **19:**2451-2461.
745
746 Shindou, H., and T. Shimizu. 2009. Acyl-CoA:lysophospholipid acyltransferases. *J. Biol. Chem*.
747 **284:**1-5.

748 Showalter MR, Berg AL, Nagourney A, Heil H, Carraway KL 3rd, Fiehn O. 2020. The emerging
749 and diverse roles of bis(monoacylglycero) phosphate lipids in cellular physiology and disease.
750 *Int. J. Mol. Sci.* **21:**8067.
751
752 Stickel F, S. Buch HD, Nischalke, KH, Weiss D, Gotthardt J, Fischer J, Rosendahl A,
753 Marot M, Elamly M, Casper F, Lammert A, McQuillin S, Zopf U, Spengler S, Marhenke MM,
754 Kirstein A, Vogel F, Eyer J, von Felden H, Wege T, Buch C, Schafmayer F, Braun P, Deltenre
755 T, Berg M, Morgan Y, Hampe J. 2018. Genetic variants in PNPLA3 and TM6SF2 predispose to
756 the development of hepatocellular carcinoma in individuals with alcohol-related cirrhosis. *Am.*
757 *J. Gastroenterol.* **113:**1475-1483.
758
759 TanakaY, Shimanaka Y, Caddeo A, Kubo T, Mao Y, Kubota T, Kubota N, Yamauchi T,
760 Mancina RM, Baselli G, Luukkonen P, Pihlajamäki J, Yki-Järvinen H, Valenti L, Arai H, Romeo
761 S, Kono N. 2021. LPIAT1/MBOAT7 depletion increases triglyceride synthesis fueled by high
762 phosphatidylinositol turnover. *Gut* **70:**180-193.
763
764 Teo K, Abeysekera KWM, Adams L, Aigner E, Anstee QM, Banales JM, Banerjee R, Basu P,
765 Berg T, Bhatnagar P, Buch S, Canbay A, Caprio S, Chatterjee A, Ida Chen JD, Chowdhury A,
766 Daly AK, Datz C, de Gracia Hahn D, DiStefano JK, et al. 2021. rs641738C>T near MBOAT7 is
767 associated with liver fat, ALT and fibrosis in NAFLD: A meta-analysis. *J. Hepatol.* **74:**20-30.
768
769 Thabet K, Asimakopoulos A, Shojaei M, Romero-Gomez M, Mangia A, Irving WL, Berg T, Dore
770 GJ, Gronbaek H, Sheridan D, Abate ML, Bugianesi E, Weltman M, Mollison L, Cheng W,
771 Riordan S, Fischer J, Spengler U, Nattermann J, Wahid A, et al. 2016. MBOAT7 rs641738
772 increases risk of liver inflammation and transition to fibrosis in chronic hepatitis C. *Nat.*
773 *Commun.* **7:**12757.
774
775 Thabet K, Chan HLY, Petta S, Mangia A, Berg T, Boonstra A, Brouwer WP, Abate ML, Wong
776 VW, Nazmy M, Fischer J, Liddle C, George J, Eslam M. 2017. The membrane-bound O-
777 acyltransferase domain-containing 7 variant rs641738 increases inflammation and fibrosis in
778 chronic hepatitis B. *Hepatology* **65:**1840-1850.
779
780 Thangapandi VR, Knittelfelder O, Brosch M, Patsenker E, Vvedenskaya O, Buch S, Hinz S,
781 Hendricks A, Nati M, Herrmann A, Rekhade DR, Berg T, Matz-Soja M, Huse K, Klipp E,
782 Pauling JK, Wodke JA, Miranda Ackerman J, Bonin MV, Aigner E. et al. 2021. Loss of hepatic
783 *Mboat7* leads to liver fibrosis. *Gut* **70:** 940-950.

Warrier, M., Warrier M, Shih DM, Burrows AC, Ferguson D, Gromovsky AD, Brown AL, Marshall S, McDaniel A, Schugar RC, Wang Z, Sacks J, Rong X, Vallim TA, Chou J, Ivanova PT, Myers DS, Brown HA, Lee RG, Crooke RM, Graham MJ, Liu X, Parini P, Tontonoz P, Lusis AJ, Hazen SL, Temel RE, Brown JM. 2015. The TMAO-Generating Enzyme Flavin Monooxygenase 3 Is a Central Regulator of Cholesterol Balance. *Cell Rep.* **10:**1-13.

Wymann, M.P., and R. Schneiter. 2008. Lipid signaling in disease. *Nat. Rev. Mol. Cell Biol.* **9:**162-176.

Xia M, Chandrasekaran P, Rong S, Fu X, Mitsche MA. 2021. Hepatic deletion of *Mboat7* (LPIAT1) causes activation of SREBP-1c and fatty liver. *J. Lipid Res.* **62:**100031.

Zarini S, Hankin JA, Murphy RC, Gijón MA. 2014. Lysophospholipid acyltransferases and arachidonate recycling in human neutrophils. *Prostaglandins Other Lipid Mediat*. **113-115:**52-61.

Zhang, Y., T. Guo, F. Yang, Y. Mao, L. Li, C. Liu, Q. Sun, Y. Li, and J. Huang. 2018. Single nucleotide rs738409 polymorphisms in the PNPLA3 gene are strongly associated with alcoholic liver disease in Han Chinese males. *Hepatol. Int.* **12:** 429-437.

818 **FIGURE LEGENDS**

819

820 **Figure 1. MBOAT7 Products Are Selectively Reduced in Heavy Drinkers.** Plasma
821 lysophosphatidylinositol (LPI - inset graph) and phosphatidylinositol (PI) species from both
822 male and female healthy controls and heavy drinkers were measured by liquid chromatography-
823 tandem mass spectrometry (LC-MS/MS). n=10-16; ***p<0.001 and ****p<0.0001 in figure 1. ANOVA
824 with Tukey's post-hoc test.

825

826 **Figure 1 – figure supplement 1.** Demographic and clinical parameters for the entire cohort of
827 healthy controls and heavy drinkers recruited for this study.

828

829 **Figure 2. Hepatocyte-Specific Deletion of *Mboat7* Promotes Ethanol-Induced Liver**
830 **Injury.** Female control (*Mboat7*$^{fl/fl}$) or hepatocyte-specific *Mboat7* knockout mice (*Mboat7*^{HSKO})
831 were fed with subjected the NIAAA model of ethanol-induced liver injury. (A) Hepatic *Mboat7*
832 expression was measured via qPCR. (B) Western blot for hepatic microsomal MBOAT7 protein
833 levels replicated in n=3 mice. (C) Liver weight, (D) Plasma alanine aminotransferase (ALT), (E)
834 Percent steatosis quantified by a blinded board-certified pathologist, (F) Hepatic triglycerides,
835 (G) Hepatic expression of Inflammatory gene measured by qPCR. n = 5-7; Data represent the
836 mean ± S.E.M. and groups not sharing a common letter superscript differ significantly (p≤0.05).

837

838 **Figure 2 – figure supplement 1. Myeloid-Specific Deletion of *Mboat7* Does not Promote**
839 **Ethanol-Induced Liver Injury.** Female control (Mboat7$^{fl/fl}$) or myeloid-specific *Mboat7*
840 knockout mice (*Mboat7*^{MSKO}) were subjected to the NIAAA model of ethanol-induced liver
841 injury. (A) Western blots from bone marrow derived macrophage (BMDM) or peritoneal
842 macrophage (PM) collected from *Mboat7*$^{fl/fl}$ or *Mboat7*^{MSKO} mice. (B) Initial and final Body

843 weight measured in *Mboat7*$^{fl/fl}$ or *Mboat7*^{MSKO} mice. (C) Liver weight (D and E) Plasma alanine
844 aminotransferase (ALT) and aspartate aminotransferase (AST). (F) Hepatic triglycerides. (G)
845 Hepatic expression of Inflammatory gene measured by qPCR. Data represent the mean ±
846 S.E.M. and groups not sharing a common letter superscript differ significantly (p≤0.05).
847
848 **Figure 3. Ethanol Alters the Liver Lipidome in a MBOAT7-Dependent Manner.** *Mboat7*$^{fl/fl}$
849 or *Mboat7*^{HSKO} mice were subjected to the NIAAA model of ethanol exposure. Liver
850 lysophosphatidylinositol (LPI) (A) and phosphatidylinositol (PI) species, including the MBOAT7
851 product PI 38:4 (B) and others (C), were quantified via liquid chromatography-tandem mass
852 spectrometry (LC-MS/MS) in (n=5-7). (D) Principal component analysis for untargeted
853 lipidomics analysis. The first and second principal components are plotted on the x- and y-
854 axes, respectively, and sample treatment group is indicated by color. (E) Heatmap showing
855 global lipidomic alterations in mouse liver. Total levels of endosomal/lysosomal lipids were
856 measured by targeted and untargeted lipidomic approach using LC-MS/MS (F) Total
857 Bis(monoacylglycero)phosphate (BMP) levels (G) Total Phosphatidylglycerol (PG) and (H)
858 Total Cardiolipin (CL) from the liver of Mboat7$^{fl/fl}$ or Mboat7^{HSKO} mice. Data represent the mean
859 ± S.E.M. and groups not sharing a common letter superscript differ significantly (p≤0.05).
860
861 **Figure 3 – figure supplement 1. Alterations in Total Hepatic Lipid Levels in *Mboat7*^{HSKO}**
862 **Mice***.* Age-matched female *Mboat7*$^{fl/fl}$ or *Mboat7*^{HSKO} mice were subjected to the NIAAA model
863 of ethanol exposure, and untargeted lipidomics was performed to broadly examine major lipid
864 classes in the liver. (A) Phosphatidylcholine (PC), (B) Phosphatidylserine (PS), (C)
865 Phosphatidylethanolamine (PE), (D) Phosphatidic acid (PA), (E) Sphingomyelins (SM), (F)
866 Ceramides (Cer), (G) Ether phosphatidylcholine, (H) Ether phosphatidylethanolamine, (I) Free
867 fatty acids (FFA), (J) Hexosylceramide (HexCer), (K) Diacylglycerol (DAG) and (L) Cholesteryl

868 ester (CE) were quantified via liquid chromatography mass spectrometry (n=6/group). Data
869 represent the mean ± S.E.M. and groups not sharing a common letter superscript differ
870 significantly (p≤0.05).
871
872 **Figure 3 – figure supplement 2. Hepatic Phosphatidylcholine (PC) Levels in *Mboat7*^{HSKO}**
873 **mice.** Age-matched female *Mboat7*$^{fl/fl}$ or *Mboat7*^{HSKO} mice were subjected to the NIAAA model
874 of ethanol exposure, and untargeted lipidomics were performed to broadly examine major lipid
875 classes in the liver. The molecular species of PC were quantified via liquid chromatography
876 mass spectrometry (n=6/group). Data represent the mean ± S.E.M. and groups not sharing a
877 common letter superscript differ significantly (p≤0.05).
878
879 **Figure 3 – figure supplement 3. Hepatic Bis(Monoacylglycerol)Phosphate (BMP) Levels**
880 **in *Mboat7*^{HSKO} mice.** Age-matched female *Mboat7*$^{fl/fl}$ or *Mboat7*^{HSKO} mice were subjected to
881 the NIAAA model of ethanol exposure, and targeted lipidomics was performed in the liver. The
882 molecular species of BMP were quantified via liquid chromatography mass spectrometry
883 (n=6/group). Data represent the mean ± S.E.M. and groups not sharing a common letter
884 superscript differ significantly (p≤0.05).
885
886 **Figure 3 – figure supplement 4. Hepatic Phosphatidylglycerol (PG) Levels in *Mboat7*^{HSKO}**
887 **mice.** Age-matched female *Mboat7*$^{fl/fl}$ or *Mboat7*^{HSKO} mice were subjected to the NIAAA model
888 of ethanol exposure, and targeted lipidomics was performed in the liver. The molecular species
889 of PG were quantified via liquid chromatography mass spectrometry (n=6/group). Data
890 represent the mean ± S.E.M. and groups not sharing a common letter superscript differ
891 significantly (p≤0.05).
892

893 **Figure 3 – figure supplement 5. Hepatic Cardiolipin (CL) Levels in *Mboat7*^{HSKO} mice.** Age-
894 matched female *Mboat7*$^{fl/fl}$ or *Mboat7*^{HSKO} mice were subjected to the NIAAA model of ethanol
895 exposure, and untargeted lipidomics was performed in the liver. The molecular species of CL
896 were quantified via liquid chromatography mass spectrometry (n=6/group). Data represent the
897 mean ± S.E.M. and groups not sharing a common letter superscript differ significantly (p≤0.05).
898
899 **Figure 3 – figure supplement 6. Hepatic Phosphatidylserine (PS) Levels in *Mboat7*^{HSKO}**
900 **mice.** Age-matched female *Mboat7*$^{fl/fl}$ or *Mboat7*^{HSKO} mice were subjected to the NIAAA model
901 of ethanol exposure, and untargeted lipidomics was performed in the liver. The molecular
902 species of PS were quantified via liquid chromatography mass spectrometry (n=6/group). Data
903 represent the mean ± S.E.M. and groups not sharing a common letter superscript differ
904 significantly (p≤0.05).
905
906 **Figure 3 – figure supplement 7. Hepatic Phosphatidylethanolamine (PE) Levels in**
907 ***Mboat7*^{HSKO} mice.** Age-matched female *Mboat7*$^{fl/fl}$ or *Mboat7*^{HSKO} mice were subjected to the
908 NIAAA model of ethanol exposure, and untargeted lipidomics was performed in the liver. The
909 molecular species of PE were quantified via liquid chromatography mass spectrometry
910 (n=6/group). Data represent the mean ± S.E.M. and groups not sharing a common letter
911 superscript differ significantly (p≤0.05).
912
913 **Figure 3 – figure supplement 8. Hepatic Phosphatidic Acid (PA) Levels in *Mboat7*^{HSKO}**
914 **mice.** Age-matched female *Mboat7*$^{fl/fl}$ or *Mboat7*^{HSKO} mice were subjected to the NIAAA model
915 of ethanol exposure, and untargeted lipidomics was performed in the liver. The molecular
916 species of PA were quantified via liquid chromatography mass spectrometry (n=6/group). Data

917 represent the mean ± S.E.M. and groups not sharing a common letter superscript differ
918 significantly (p≤0.05).
919
920 **Figure 3 – figure supplement 9. Hepatic Sphingomyelin (SM) Levels in *Mboat7*^{HSKO} mice.**
921 Age-matched female *Mboat7*$^{fl/fl}$ or *Mboat7*^{HSKO} mice were subjected to the NIAAA model of
922 ethanol exposure, and untargeted lipidomics was performed in the liver. The molecular species
923 of SM were quantified via liquid chromatography mass spectrometry (n=6/group). Data
924 represent the mean ± S.E.M. and groups not sharing a common letter superscript differ
925 significantly (p≤0.05).
926
927 **Figure 3 – figure supplement 10. Hepatic Ceramide (Cer) Levels in *Mboat7*^{HSKO} mice.**
928 Age-matched female *Mboat7*$^{fl/fl}$ or *Mboat7*^{HSKO} mice were subjected to the NIAAA model of
929 ethanol exposure, and untargeted lipidomics was performed in the liver. The molecular species
930 of ceramides were quantified via liquid chromatography mass spectrometry (n=6/group). Data
931 represent the mean ± S.E.M. and groups not sharing a common letter superscript differ
932 significantly (p≤0.05).
933
934 **Figure 3 – figure supplement 11. Hepatic Ether-Linked Lipids Levels in *Mboat7*^{HSKO} mice.**
935 Age-matched female *Mboat7*$^{fl/fl}$ or *Mboat7*^{HSKO} mice were subjected to the NIAAA model of
936 ethanol exposure, and untargeted lipidomics was performed in the liver. The molecular species
937 of ether-linked lipids were quantified via liquid chromatography mass spectrometry
938 (n=6/group). Data represent the mean ± S.E.M. and groups not sharing a common letter
939 superscript differ significantly (p≤0.05).
940
941 **Figure 4. *Mboat7*^{HSKO} Mice Have Dysregulated Lysosome Function in Response to**

942 **Ethanol.** Age-matched female *Mboat7*$^{fl/fl}$ or *Mboat7*^{HSKO} mice were subjected to the NIAAA
943 model of ethanol exposure**.** (A) Total liver lysates were subjected to western blot analysis of
944 major autophagy marker genes (LC3A/B, P62), mTOR and lysosome biogenesis genes
945 (TFEB, LAMP-1, LAMP-2 and ATP6V1A). (B) Nuclear fractions from mouse livers of Mboat7$^{fl/fl}$
946 and *Mboat7*^{HSKO} were subjected to western blot analysis of TFEB. (C) Lysosome protein
947 degradation activity in wild type and MBOAT7Δ-Huh7 hepatoma cells treated with or without
948 100 mM ethanol for 48 h was assessed by incubating cells with 10 μg/mL of lysosome
949 indicator for 2 h and examined by flow cytometry. (n=5 from two experiments by normalizing to
950 wild type group in each experiment; mean ± S.D. (D) Expression levels of the genes encoding
951 functions in lysosomal hydrolase and accessory, lysosomal m involved in lysosomal
952 biogenesis in the liver of Mboat7$^{fl/fl}$ and Mboat7^{HSKO} *mice* upon ethanol feeding. mRNA
953 expression levels were determined by qPCR. (n=6/group). Groups not sharing a common letter
954 superscript differ significantly (p≤0.05).
955
956 **Figure 4 – figure supplement 1. Genetic Deletion of MBOAT7 in Human Huh7 Cells is**
957 **Associated with Diminished Lysosome Biogenesis and Ethanol-Induced Autophagy**
958 **Dysregulation.** WT and *MBOAT7Δ* Huh7 hepatoma cells were treated with and without
959 ethanol treatment (100mM) for 24 (A) and 48h (B). Total lysate were subjected to western blot
960 analysis of LC3A/B, P62, Total mTOR, Total TFEB, LAMP-1, LAMP-2 and ATP6V1A.
961
962 **Figure 4 – figure supplement 2. Working Model.** MBOAT7 loss of function in either mouse
963 or human hepatocytes is associated with decreased TFEB-driven lysosomal biogenesis and
964 defective autophagy secondary to lysosomal dysfunction.
965
966
967

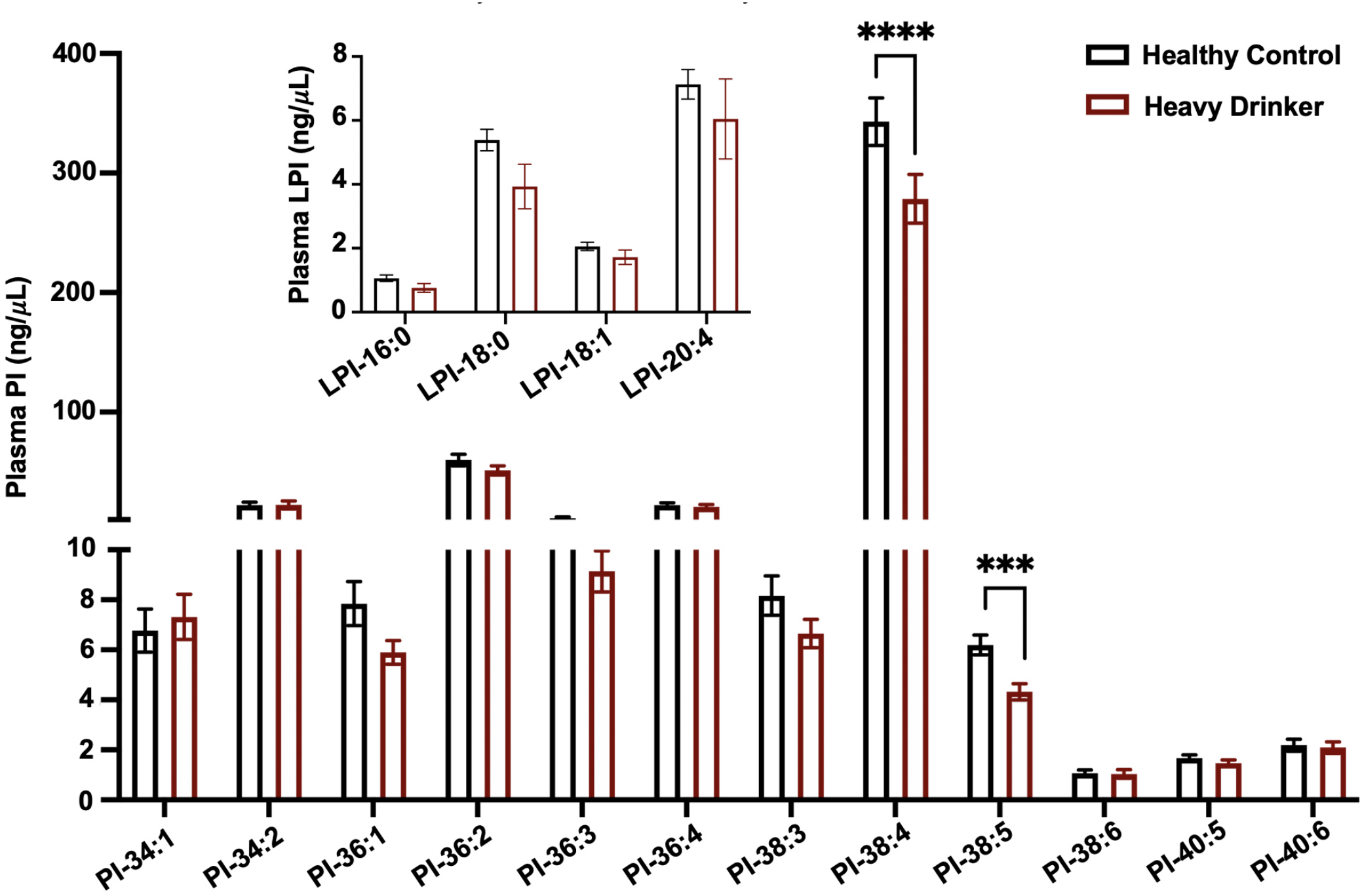
Healthy Control
Heavy Drinker
Plasma PI (ng/μL)
400
300
200
100
10
8
6
4
2
0
****
***
Plasma LPI (ng/μL)
8
6
4
2
0
LPI-16:0
LPI-18:0
LPI-18:1
LPI-20:4
PI-34:1
PI-34:2
PI-36:1
PI-36:2
PI-36:3
PI-36:4
PI-38:3
PI-38:4
PI-38:5
PI-38:6
PI-40:5
PI-40:6

DASH MBOAT7 Clinical Demographics for Healthy Control vs Heavy Drinkers

	Healthy Control (N=25)	Heavy Drinker (N=21)	Total (N=46)	p value
Sex				0.88
Female	16 (64.0%)	13 (61.9%)	29 (63.0%)	
Male	9 (36.0%)	8 (38.1%)	17 (37.0%)	
Age				0.85
Mean	45.16	44.38	44.80	
Range	23.00 - 63.00	21.00 - 63.00	21.00 - 63.00	
Race				0.06
African American	5 (20.0%)	13 (61.9%)	18 (39.1%)	
Asian	1 (4.0%)	0 (0.0%)	1 (2.2%)	
Hispanic	1 (4.0%)	1 (4.8%)	2 (4.3%)	
Unknown	3 (12.0%)	1 (4.8%)	4 (8.7%)	
White	15 (60.0%)	6 (28.6%)	21 (45.7%)	
BMI				0.03
Mean	27.12	23.83	24.74	
Range	22.12 - 30.90	15.16 - 28.59	15.16 - 30.90	
Bilirubin				0.14
Mean	0.57	0.79	0.72	
Range	0.20 - 0.90	0.10 - 1.60	0.10 - 1.60	
AST				0.51
Mean	24.56	26.52	25.93	
Range	16.00 - 38.00	15.00 - 44.00	15.00 - 44.00	
ALT				0.98
Mean	23.22	23.10	23.13	
Range	12.00 - 41.00	10.00 - 59.00	10.00 - 59.00	
Creatine				0.94
Mean	0.91	0.90	0.90	
Range	0.51 - 1.20	0.41 - 1.68	0.41 - 1.68	
INR				0.90
Mean	1.06	1.05	1.05	
Range	1.00 - 1.14	0.96 - 1.13	0.96 - 1.14	
Albumin				0.13
Mean	3.41	4.03	3.86	
Range	0.51 - 4.70	3.50 - 4.70	0.51 - 4.70	
Total Protein				0.97
Mean	6.90	6.91	6.91	
Range	6.20 - 7.30	5.50 - 8.30	5.50 - 8.30	
Globulin				< 0.01
Mean	13.50	5.48	7.56	
Range	9.80 - 16.00	1.80 - 14.40	1.80 - 16.00	

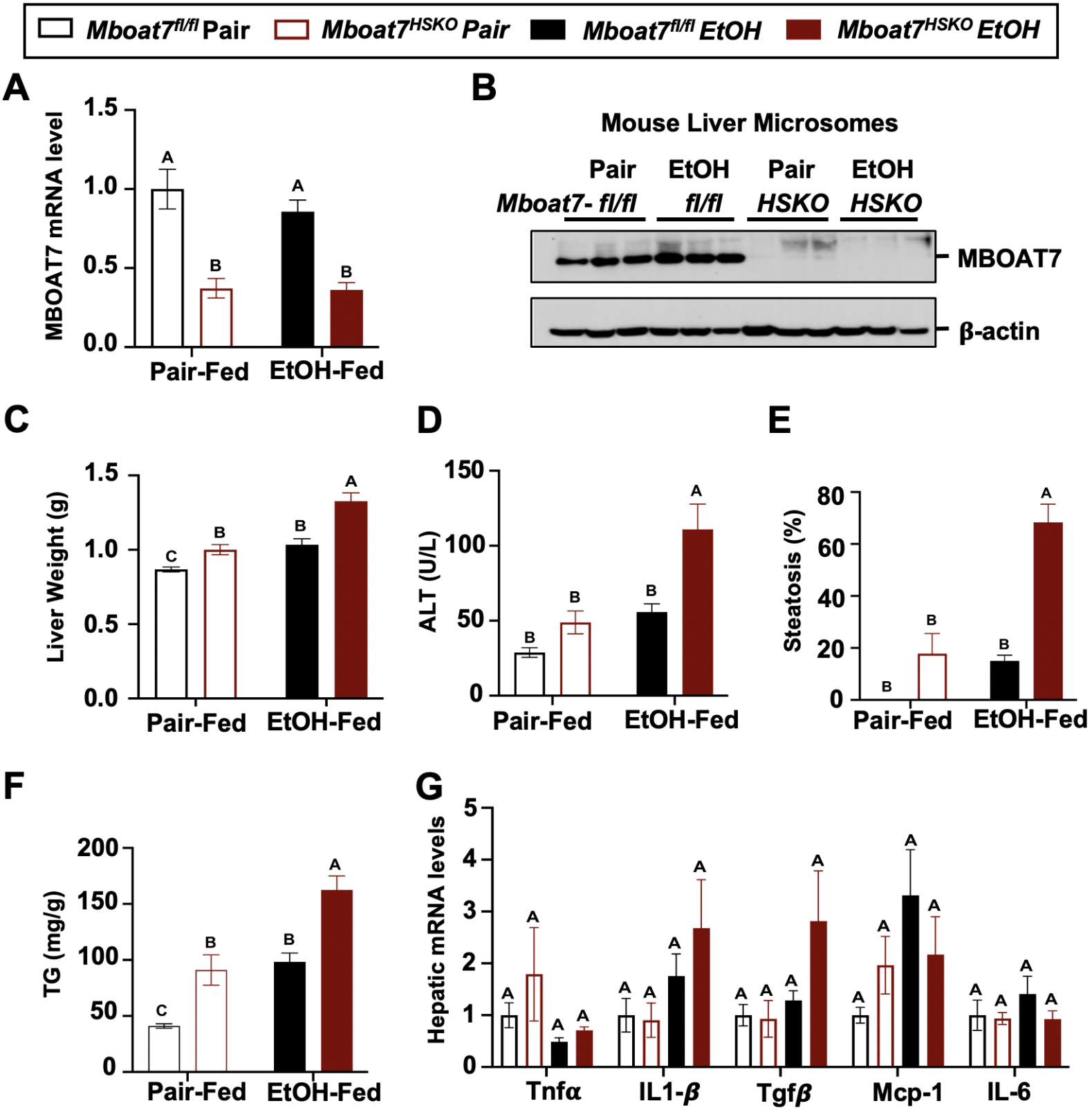
Mboat7fl/fl Pair
Mboat7HSKO Pair
Mboat7fl/fl EtOH
Mboat7HSKO EtOH
A
MBOAT7 mRNA level
1.5
1.0
0.5
0.0
Pair-Fed
EtOH-Fed
B
Mouse Liver Microsomes
Pair
EtOH
Pair
EtOH
Mboat7- fl/fl
fl/fl
HSKO
HSKO
MBOAT7
β-actin
C
Liver Weight (g)
D
ALT (U/L)
150
100
50
0
E
Steatosis (%)
80
60
40
20
0
F
TG (mg/g)
200
150
100
50
0
G
Hepatic mRNA levels
5
4
3
2
1
0
Tnfα
IL1-β
Tgfβ
Mcp-1
IL-6

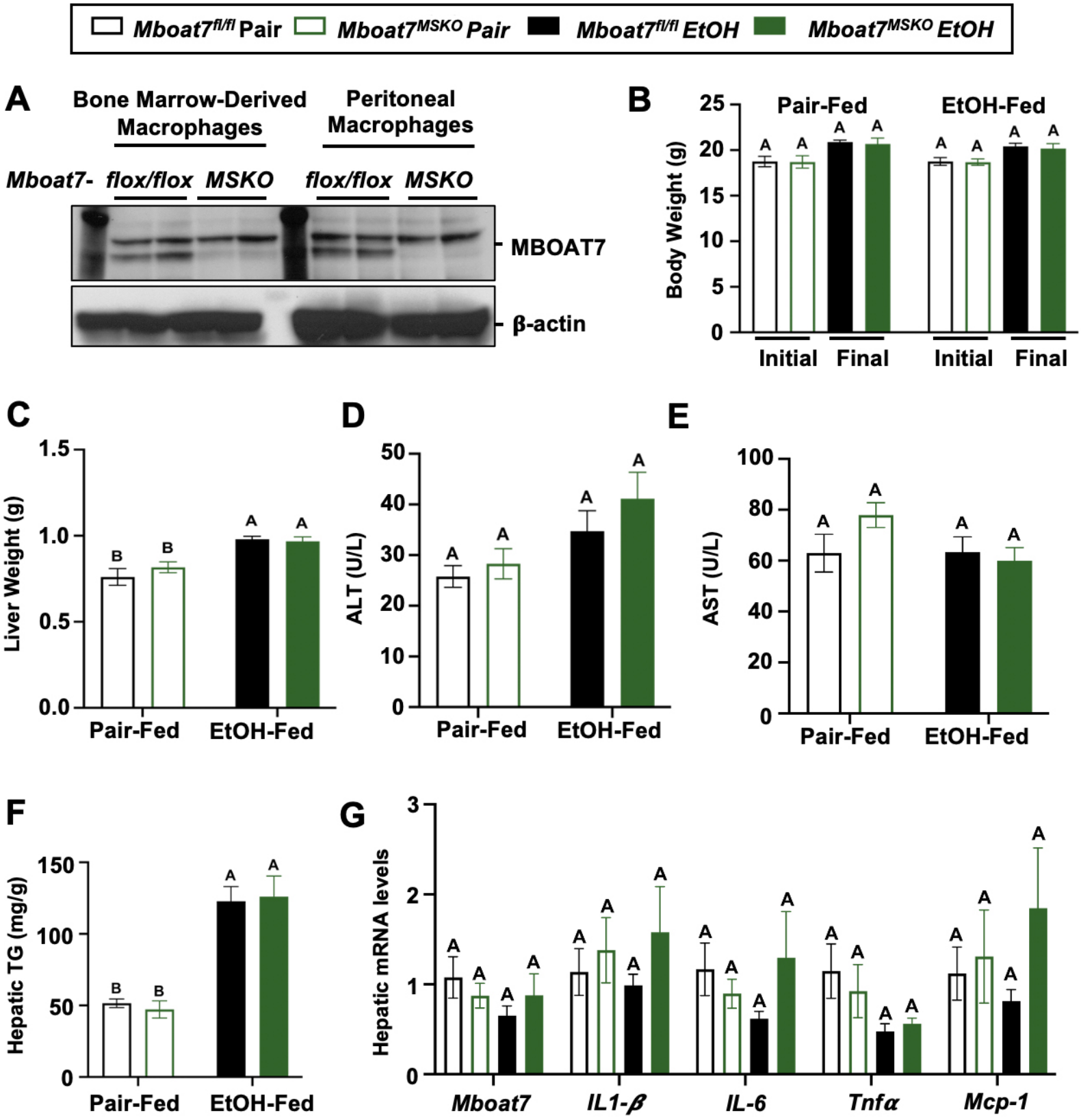
Mboat7fl/fl Pair
Mboat7MSKO Pair
Mboat7fl/fl EtOH
Mboat7MSKO EtOH
A
Bone Marrow-Derived Macrophages
Peritoneal Macrophages
Mboat7-
flox/flox
MSKO
flox/flox
MSKO
MBOAT7
β-actin
B
Pair-Fed
EtOH-Fed
Body Weight (g)
Initial
Final
Initial
Final
C
Liver Weight (g)
Pair-Fed
EtOH-Fed
D
ALT (U/L)
Pair-Fed
EtOH-Fed
E
AST (U/L)
Pair-Fed
EtOH-Fed
F
Hepatic TG (mg/g)
Pair-Fed
EtOH-Fed
G
Hepatic mRNA levels
Mboat7
IL1-β
IL-6
Tnfα
Mcp-1

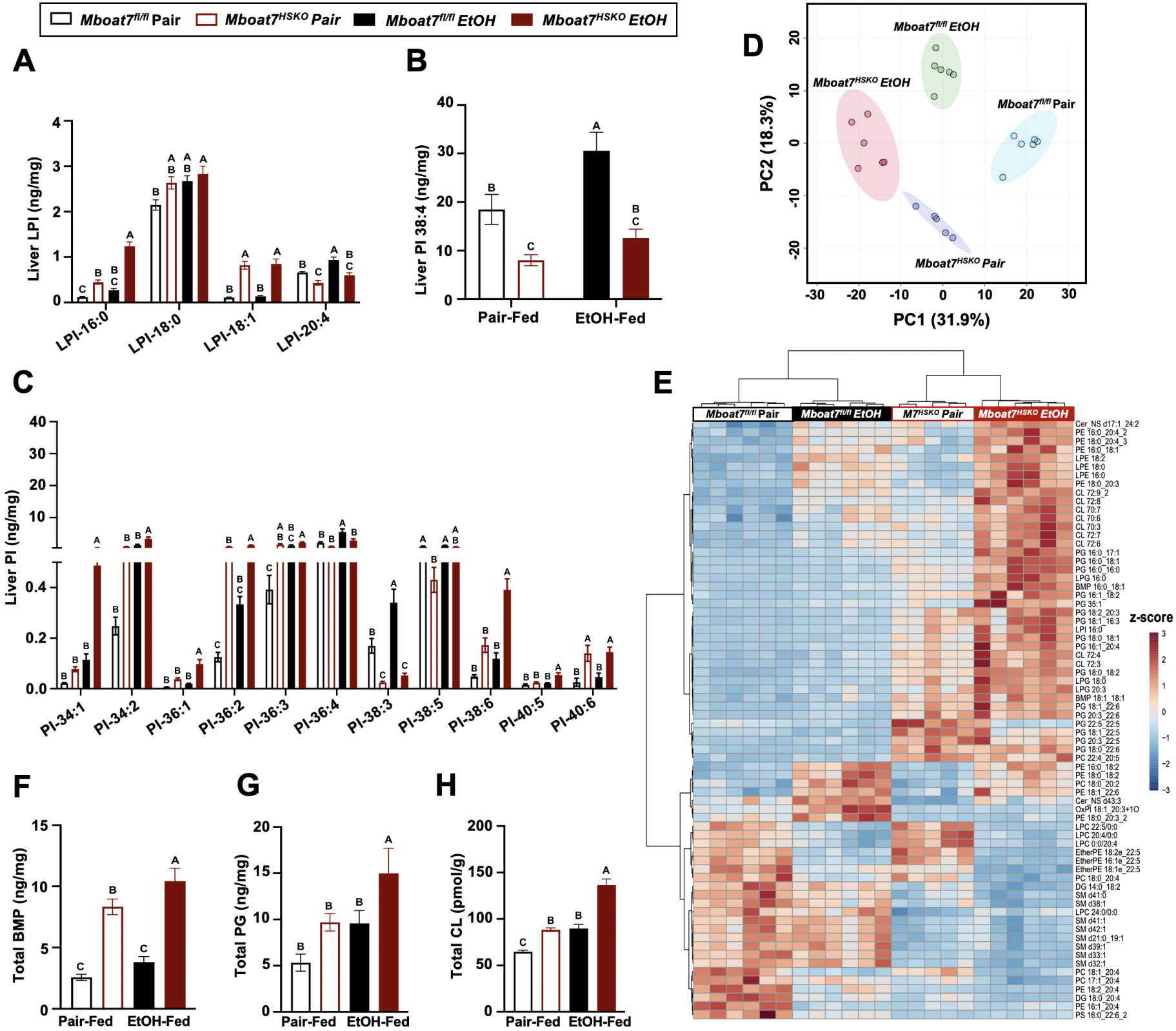
Mboat7fl/fl Pair
Mboat7HSKO Pair
Mboat7fl/fl EtOH
Mboat7HSKO EtOH
A
Liver LPI (ng/mg)
LPI-16:0
LPI-18:0
LPI-18:1
LPI-20:4
B
Liver PI 38:4 (ng/mg)
Pair-Fed
EtOH-Fed
D
PC2 (18.3%)
PC1 (31.9%)
Mboat7fl/fl EtOH
Mboat7HSKO EtOH
Mboat7fl/fl Pair
Mboat7HSKO Pair
C
Liver PI (ng/mg)
PI-34:1
PI-34:2
PI-36:1
PI-36:2
PI-36:3
PI-36:4
PI-38:3
PI-38:5
PI-38:6
PI-40:5
PI-40:6
E
Mboat7fl/fl Pair
Mboat7fl/fl EtOH
M7HSKO Pair
Mboat7HSKO EtOH
z-score
F
Total BMP (ng/mg)
Pair-Fed
EtOH-Fed
G
Total PG (ng/mg)
Pair-Fed
EtOH-Fed
H
Total CL (pmol/g)
Pair-Fed
EtOH-Fed

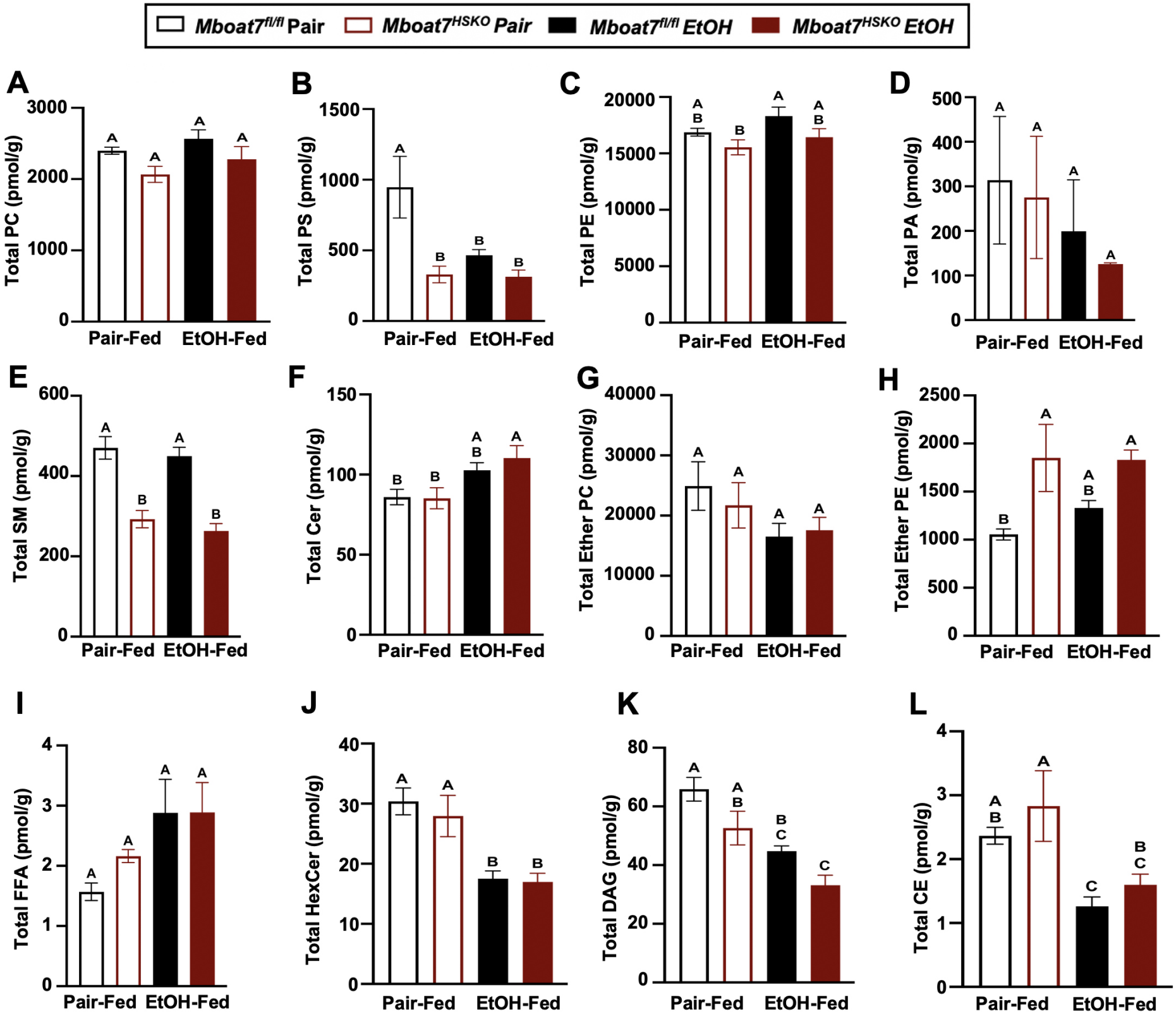
Mboat7fl/fl Pair
Mboat7HSKO Pair
Mboat7fl/fl EtOH
Mboat7HSKO EtOH
A
Total PC (pmol/g)
Pair-Fed
EtOH-Fed
B
Total PS (pmol/g)
C
Total PE (pmol/g)
D
Total PA (pmol/g)
E
Total SM (pmol/g)
F
Total Cer (pmol/g)
G
Total Ether PC (pmol/g)
H
Total Ether PE (pmol/g)
I
Total FFA (pmol/g)
J
Total HexCer (pmol/g)
K
Total DAG (pmol/g)
L
Total CE (pmol/g)

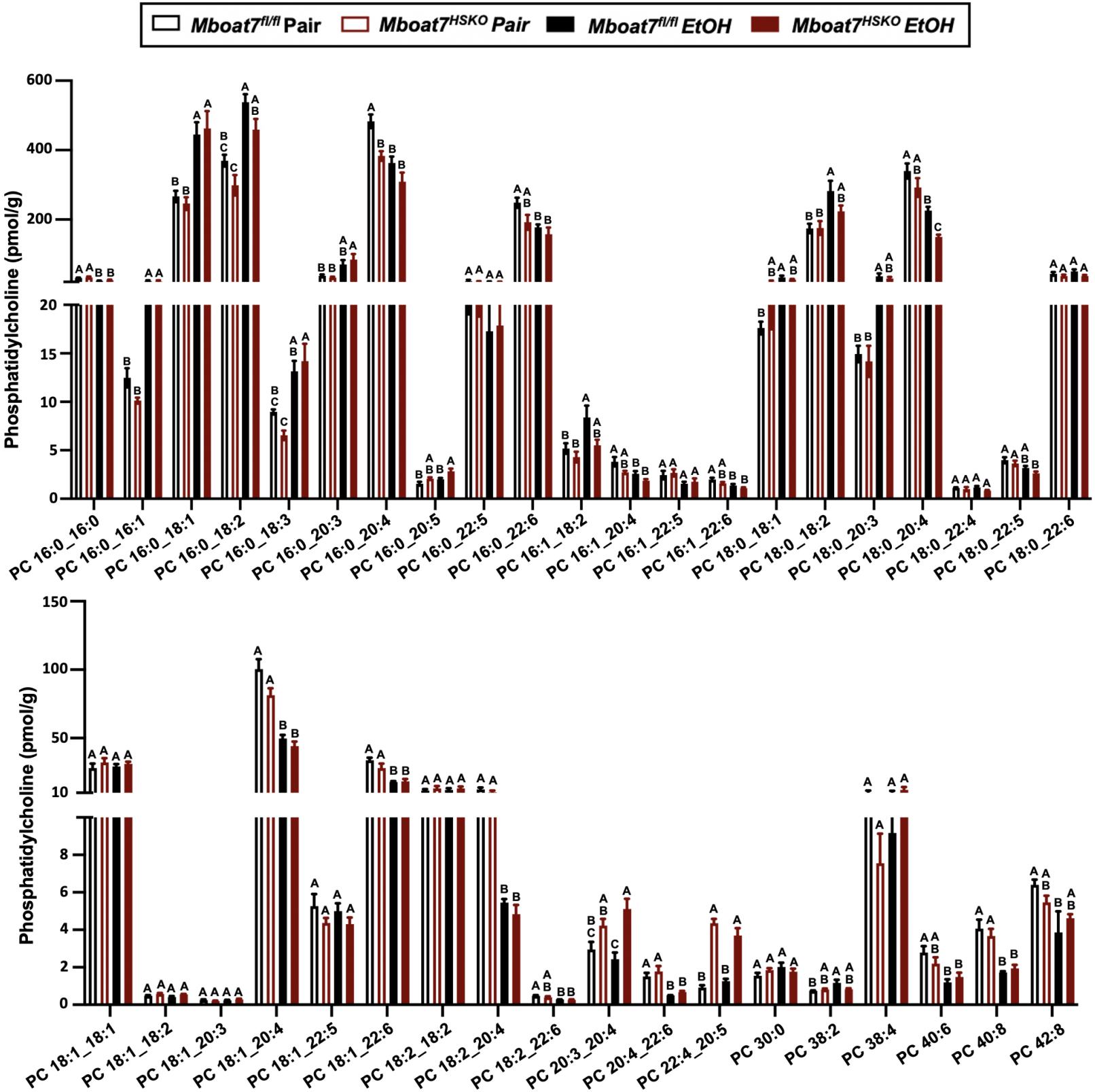
Mboat7fl/fl Pair
Mboat7HSKO Pair
Mboat7fl/fl EtOH
Mboat7HSKO EtOH
Phosphatidylcholine (pmol/g)
PC 16:0_16:0
PC 16:0_16:1
PC 16:0_18:1
PC 16:0_18:2
PC 16:0_18:3
PC 16:0_20:3
PC 16:0_20:4
PC 16:0_20:5
PC 16:0_22:5
PC 16:0_22:6
PC 16:1_18:2
PC 16:1_20:4
PC 16:1_22:5
PC 16:1_22:6
PC 18:0_18:1
PC 18:0_18:2
PC 18:0_20:3
PC 18:0_20:4
PC 18:0_22:4
PC 18:0_22:5
PC 18:0_22:6
Phosphatidylcholine (pmol/g)
PC 18:1_18:1
PC 18:1_18:2
PC 18:1_20:3
PC 18:1_20:4
PC 18:1_22:5
PC 18:1_22:6
PC 18:2_18:2
PC 18:2_20:4
PC 18:2_22:6
PC 20:3_20:4
PC 20:4_22:6
PC 22:4_20:5
PC 30:0
PC 38:2
PC 38:4
PC 40:6
PC 40:8
PC 42:8

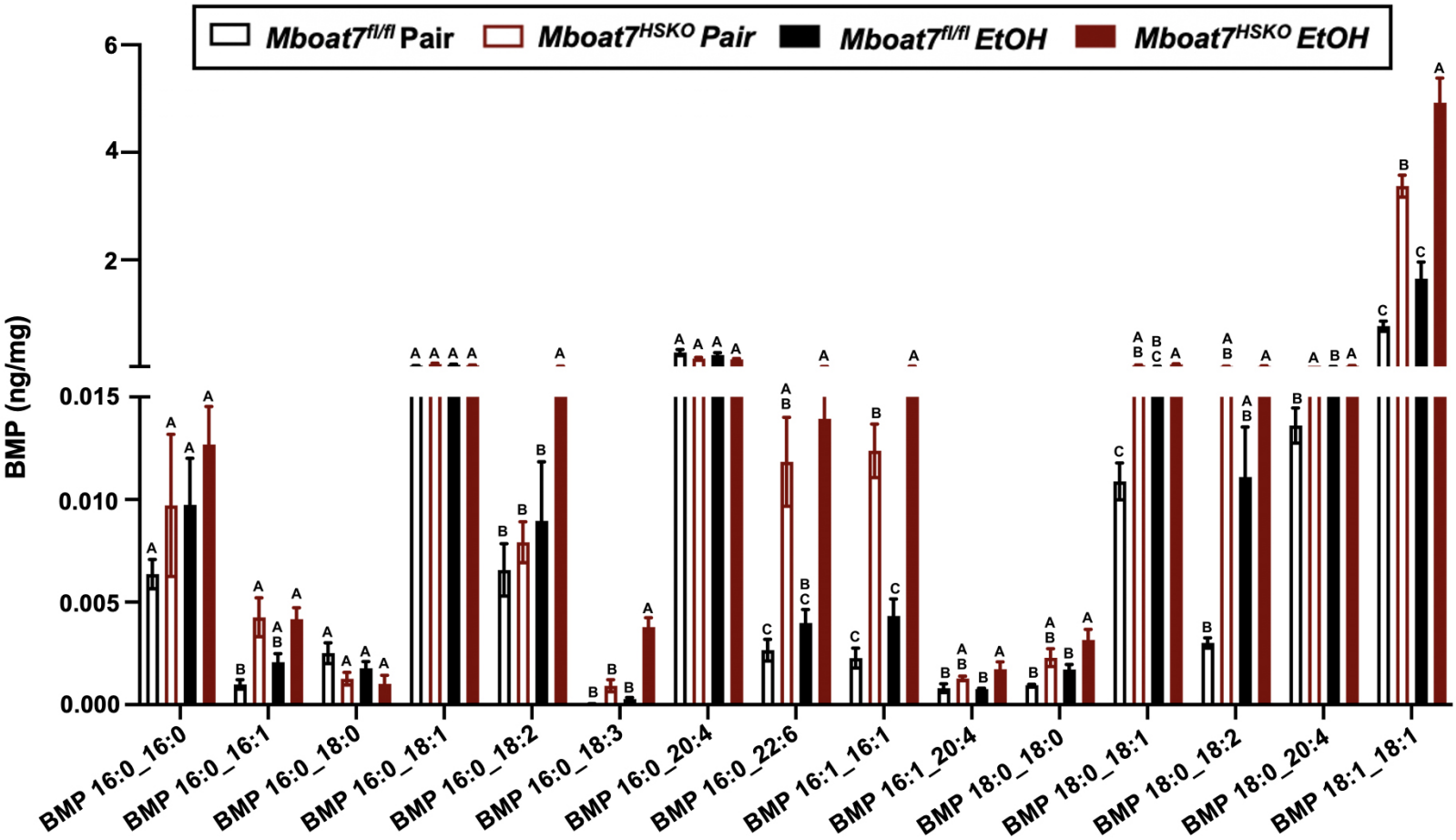
Mboat7fl/fl Pair
Mboat7HSKO Pair
Mboat7fl/fl EtOH
Mboat7HSKO EtOH
BMP (ng/mg)
BMP 16:0_16:0
BMP 16:0_16:1
BMP 16:0_18:0
BMP 16:0_18:1
BMP 16:0_18:2
BMP 16:0_18:3
BMP 16:0_20:4
BMP 16:0_22:6
BMP 16:1_16:1
BMP 16:1_20:4
BMP 18:0_18:0
BMP 18:0_18:1
BMP 18:0_18:2
BMP 18:0_20:4
BMP 18:1_18:1

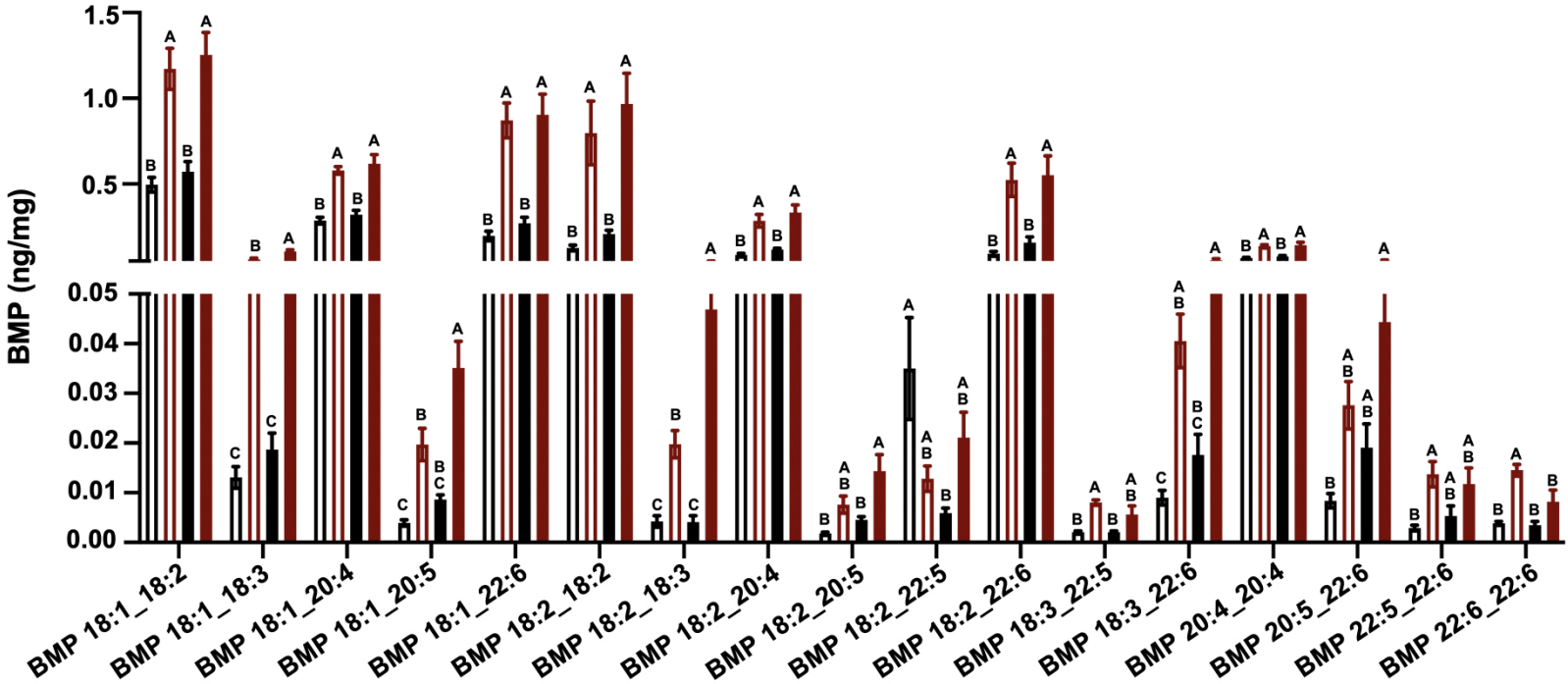
BMP (ng/mg)
BMP 18:1_18:2
BMP 18:1_18:3
BMP 18:1_20:4
BMP 18:1_20:5
BMP 18:1_22:6
BMP 18:2_18:2
BMP 18:2_18:3
BMP 18:2_20:4
BMP 18:2_20:5
BMP 18:2_22:5
BMP 18:2_22:6
BMP 18:3_22:5
BMP 18:3_22:6
BMP 20:4_20:4
BMP 20:5_22:6
BMP 22:5_22:6
BMP 22:6_22:6

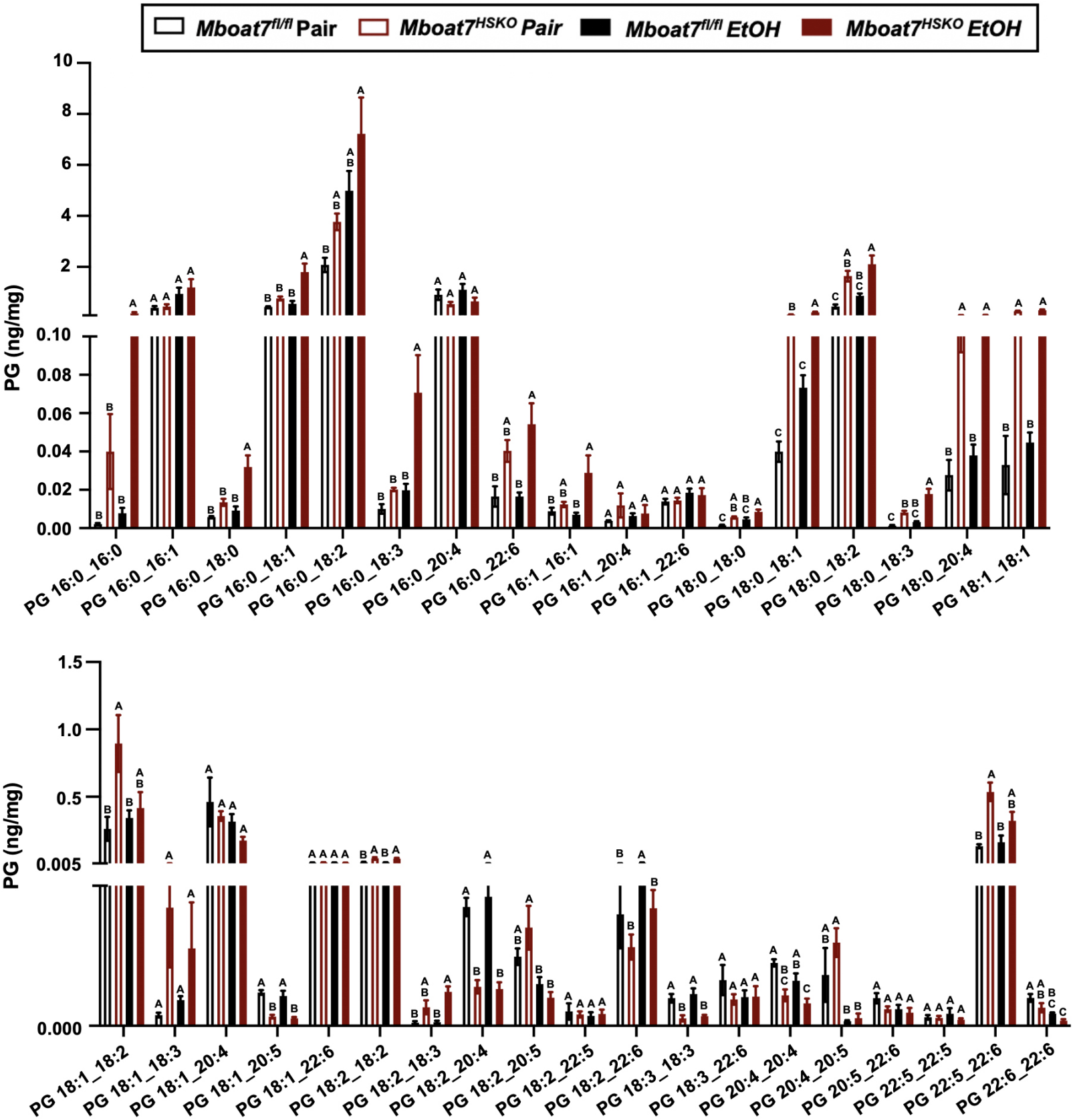
Mboat7fl/fl Pair
Mboat7HSKO Pair
Mboat7fl/fl EtOH
Mboat7HSKO EtOH
PG (ng/mg)
PG 16:0_16:0
PG 16:0_16:1
PG 16:0_18:0
PG 16:0_18:1
PG 16:0_18:2
PG 16:0_18:3
PG 16:0_20:4
PG 16:0_22:6
PG 16:1_16:1
PG 16:1_20:4
PG 16:1_22:6
PG 18:0_18:0
PG 18:0_18:1
PG 18:0_18:2
PG 18:0_18:3
PG 18:0_20:4
PG 18:1_18:1
PG 18:1_18:2
PG 18:1_18:3
PG 18:1_20:4
PG 18:1_20:5
PG 18:1_22:6
PG 18:2_18:2
PG 18:2_18:3
PG 18:2_20:4
PG 18:2_20:5
PG 18:2_22:5
PG 18:2_22:6
PG 18:3_18:3
PG 18:3_22:6
PG 20:4_20:4
PG 20:4_20:5
PG 20:5_22:6
PG 22:5_22:5
PG 22:5_22:6
PG 22:6_22:6

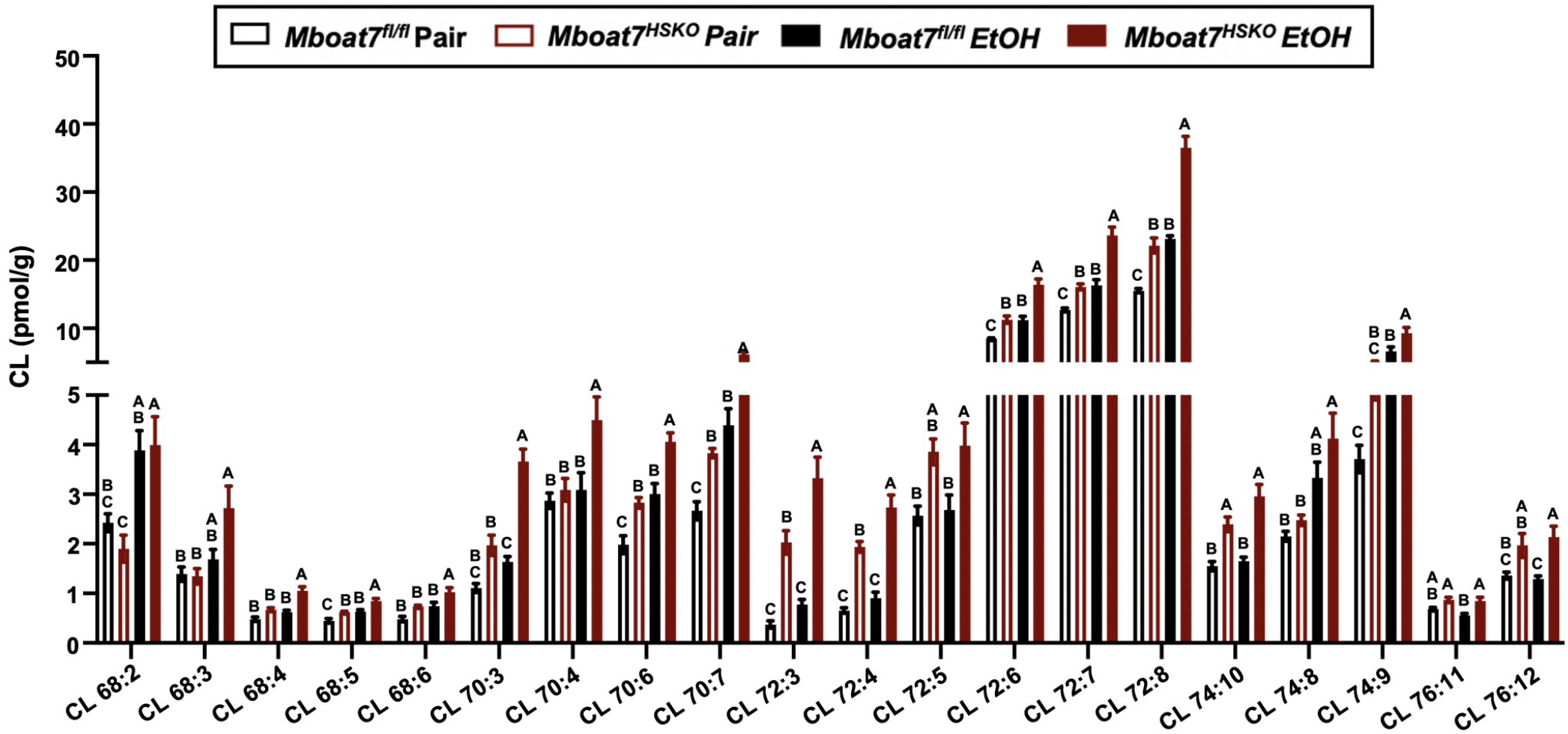
Mboat7fl/fl Pair
Mboat7HSKO Pair
Mboat7fl/fl EtOH
Mboat7HSKO EtOH
CL (pmol/g)
50
40
30
20
10
5
4
3
2
1
0
CL 68:2
CL 68:3
CL 68:4
CL 68:5
CL 68:6
CL 70:3
CL 70:4
CL 70:6
CL 70:7
CL 72:3
CL 72:4
CL 72:5
CL 72:6
CL 72:7
CL 72:8
CL 74:10
CL 74:8
CL 74:9
CL 76:11
CL 76:12

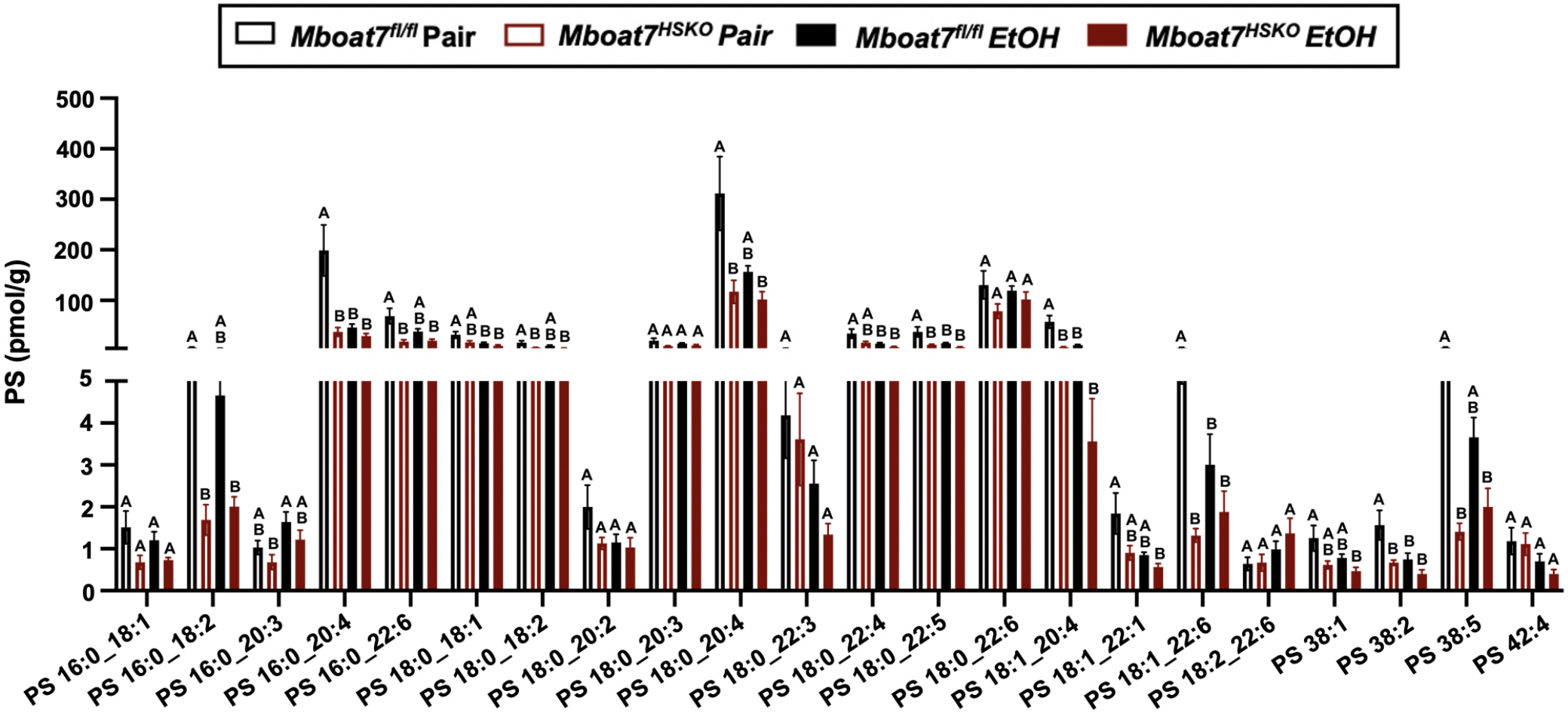
Mboat7fl/fl Pair
Mboat7HSKO Pair
Mboat7fl/fl EtOH
Mboat7HSKO EtOH
PS (pmol/g)
500
400
300
200
100
5
4
3
2
1
0
PS 16:0_18:1
PS 16:0_18:2
PS 16:0_20:3
PS 16:0_20:4
PS 16:0_22:6
PS 18:0_18:1
PS 18:0_18:2
PS 18:0_20:2
PS 18:0_20:3
PS 18:0_20:4
PS 18:0_22:3
PS 18:0_22:4
PS 18:0_22:5
PS 18:0_22:6
PS 18:1_20:4
PS 18:1_22:1
PS 18:1_22:6
PS 18:2_22:6
PS 38:1
PS 38:2
PS 38:5
PS 42:4

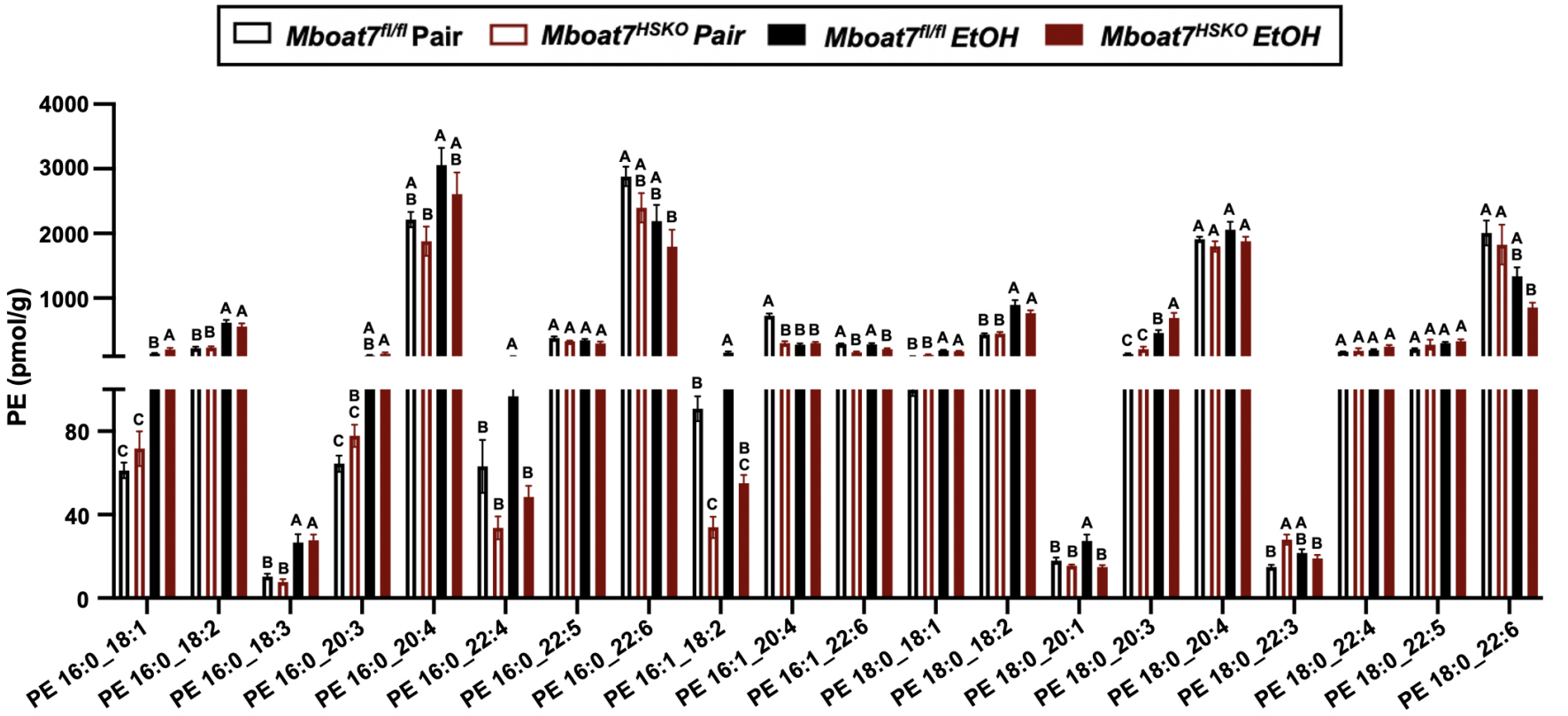
Mboat7fl/fl Pair
Mboat7HSKO Pair
Mboat7fl/fl EtOH
Mboat7HSKO EtOH
PE (pmol/g)
4000
3000
2000
1000
80
40
0
PE 16:0_18:1
PE 16:0_18:2
PE 16:0_18:3
PE 16:0_20:3
PE 16:0_20:4
PE 16:0_22:4
PE 16:0_22:5
PE 16:0_22:6
PE 16:1_18:2
PE 16:1_20:4
PE 16:1_22:6
PE 18:0_18:1
PE 18:0_18:2
PE 18:0_20:1
PE 18:0_20:3
PE 18:0_20:4
PE 18:0_22:3
PE 18:0_22:4
PE 18:0_22:5
PE 18:0_22:6

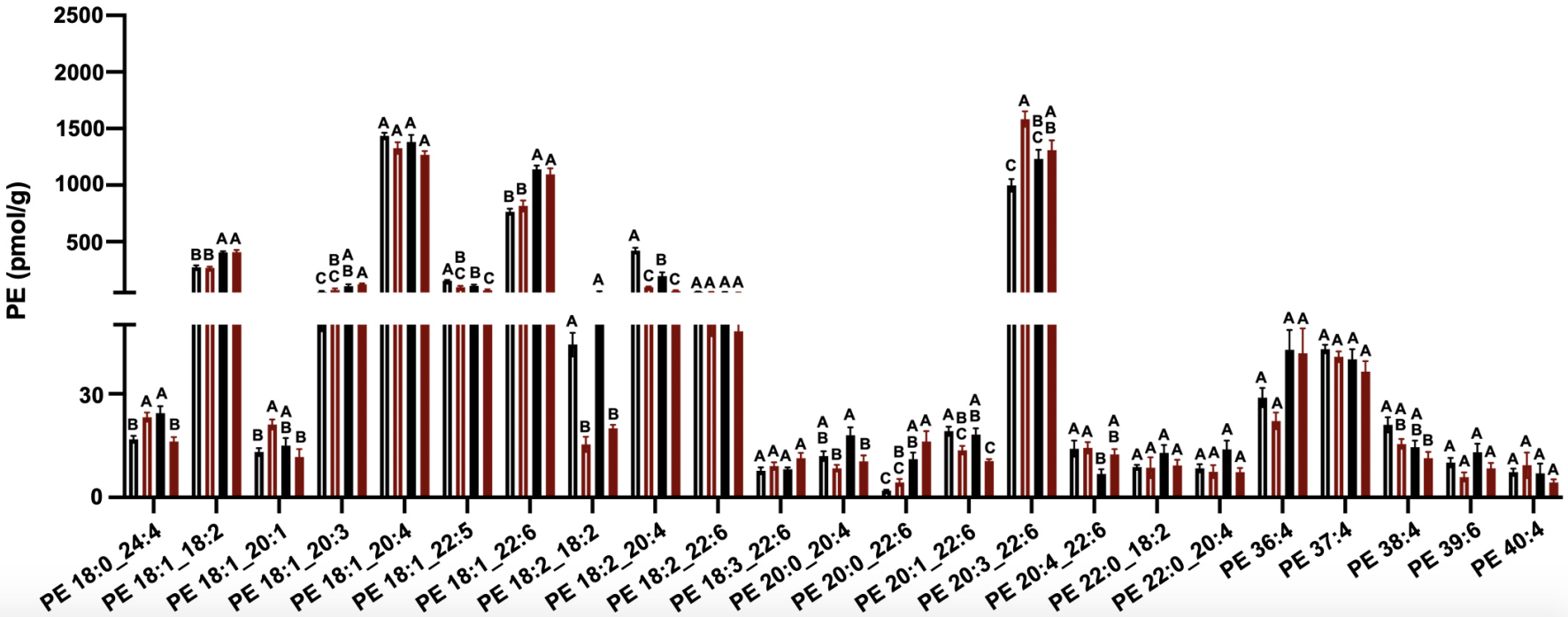
PE (pmol/g)
2500
2000
1500
1000
500
30
0
PE 18:0_24:4
PE 18:1_18:2
PE 18:1_20:1
PE 18:1_20:3
PE 18:1_20:4
PE 18:1_22:5
PE 18:1_22:6
PE 18:2_18:2
PE 18:2_20:4
PE 18:2_22:6
PE 18:3_22:6
PE 20:0_20:4
PE 20:0_22:6
PE 20:1_22:6
PE 20:3_22:6
PE 20:4_22:6
PE 22:0_18:2
PE 22:0_20:4
PE 36:4
PE 37:4
PE 38:4
PE 39:6
PE 40:4

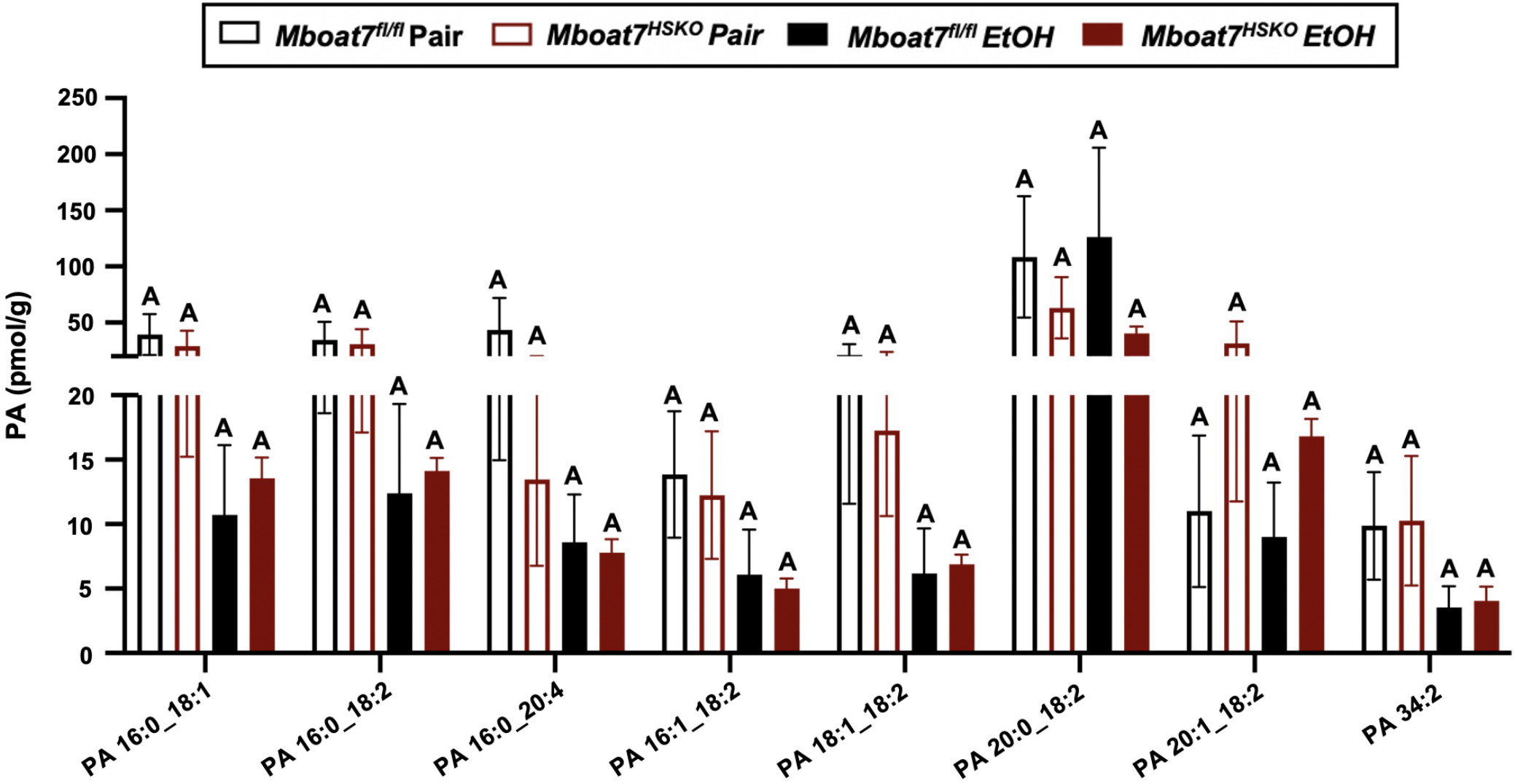
Mboat7fl/fl Pair
Mboat7HSKO Pair
Mboat7fl/fl EtOH
Mboat7HSKO EtOH
PA (pmol/g)
250
200
150
100
50
20
15
10
5
0
A
PA 16:0_18:1
PA 16:0_18:2
PA 16:0_20:4
PA 16:1_18:2
PA 18:1_18:2
PA 20:0_18:2
PA 20:1_18:2
PA 34:2

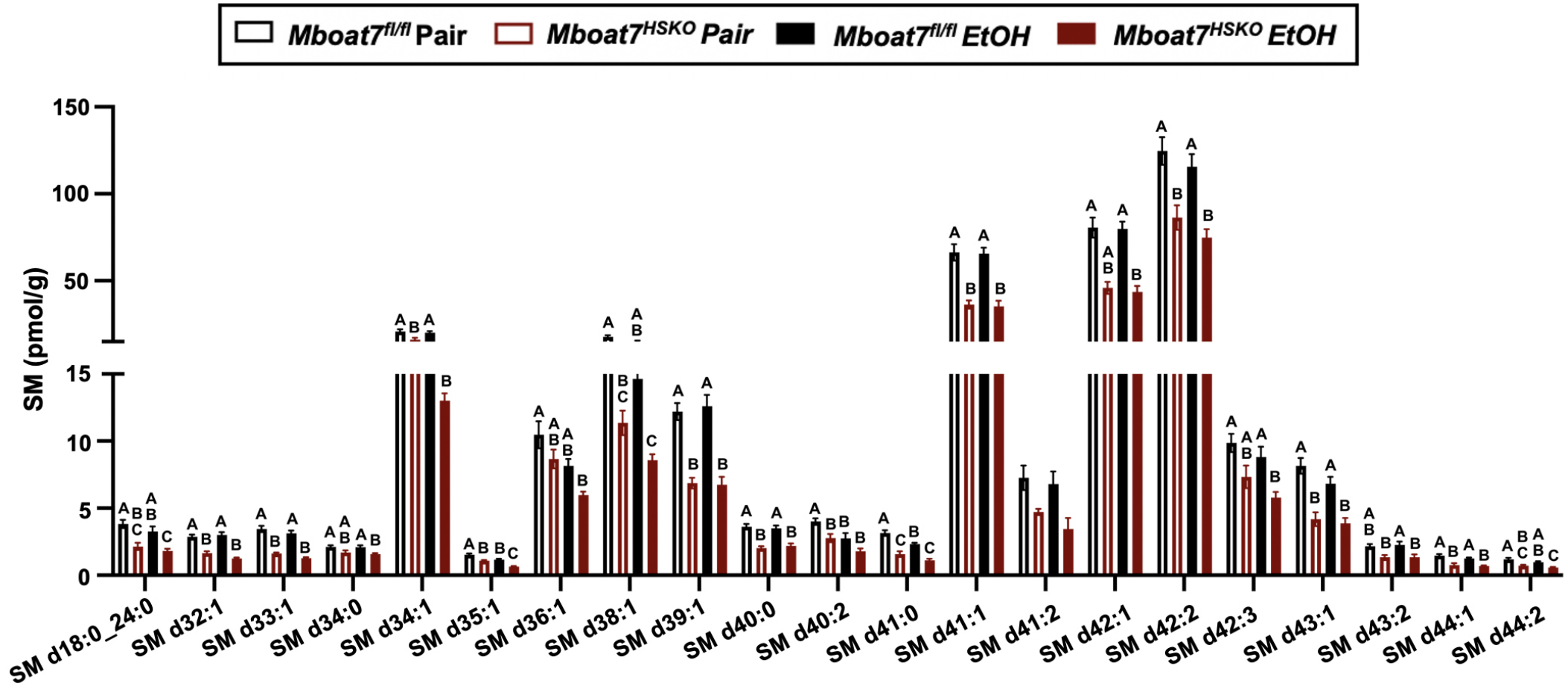
Mboat7fl/fl Pair
Mboat7HSKO Pair
Mboat7fl/fl EtOH
Mboat7HSKO EtOH
SM (pmol/g)
150
100
50
15
10
5
0
SM d18:0_24:0
SM d32:1
SM d33:1
SM d34:0
SM d34:1
SM d35:1
SM d36:1
SM d38:1
SM d39:1
SM d40:0
SM d40:2
SM d41:0
SM d41:1
SM d41:2
SM d42:1
SM d42:2
SM d42:3
SM d43:1
SM d43:2
SM d44:1
SM d44:2

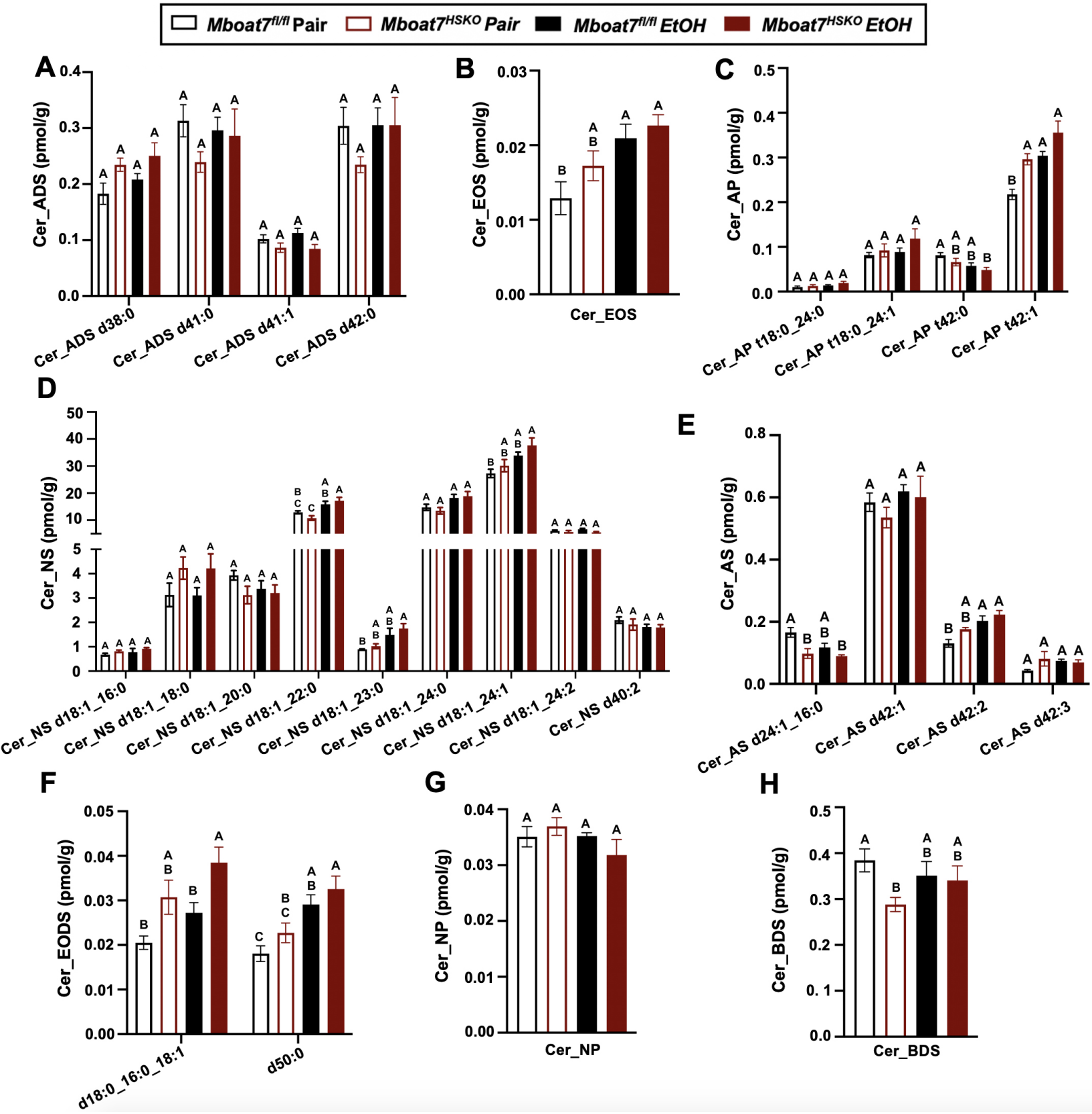
Mboat7fl/fl Pair
Mboat7HSKO Pair
Mboat7fl/fl EtOH
Mboat7HSKO EtOH
A
Cer_ADS (pmol/g)
Cer_ADS d38:0
Cer_ADS d41:0
Cer_ADS d41:1
Cer_ADS d42:0
B
Cer_EOS (pmol/g)
Cer_EOS
C
Cer_AP (pmol/g)
Cer_AP t18:0_24:0
Cer_AP t18:0_24:1
Cer_AP t42:0
Cer_AP t42:1
D
Cer_NS (pmol/g)
Cer_NS d18:1_16:0
Cer_NS d18:1_18:0
Cer_NS d18:1_20:0
Cer_NS d18:1_22:0
Cer_NS d18:1_23:0
Cer_NS d18:1_24:0
Cer_NS d18:1_24:1
Cer_NS d18:1_24:2
Cer_NS d40:2
E
Cer_AS (pmol/g)
Cer_AS d24:1_16:0
Cer_AS d42:1
Cer_AS d42:2
Cer_AS d42:3
F
Cer_EODS (pmol/g)
d18:0_16:0_18:1
d50:0
G
Cer_NP (pmol/g)
Cer_NP
H
Cer_BDS (pmol/g)
Cer_BDS

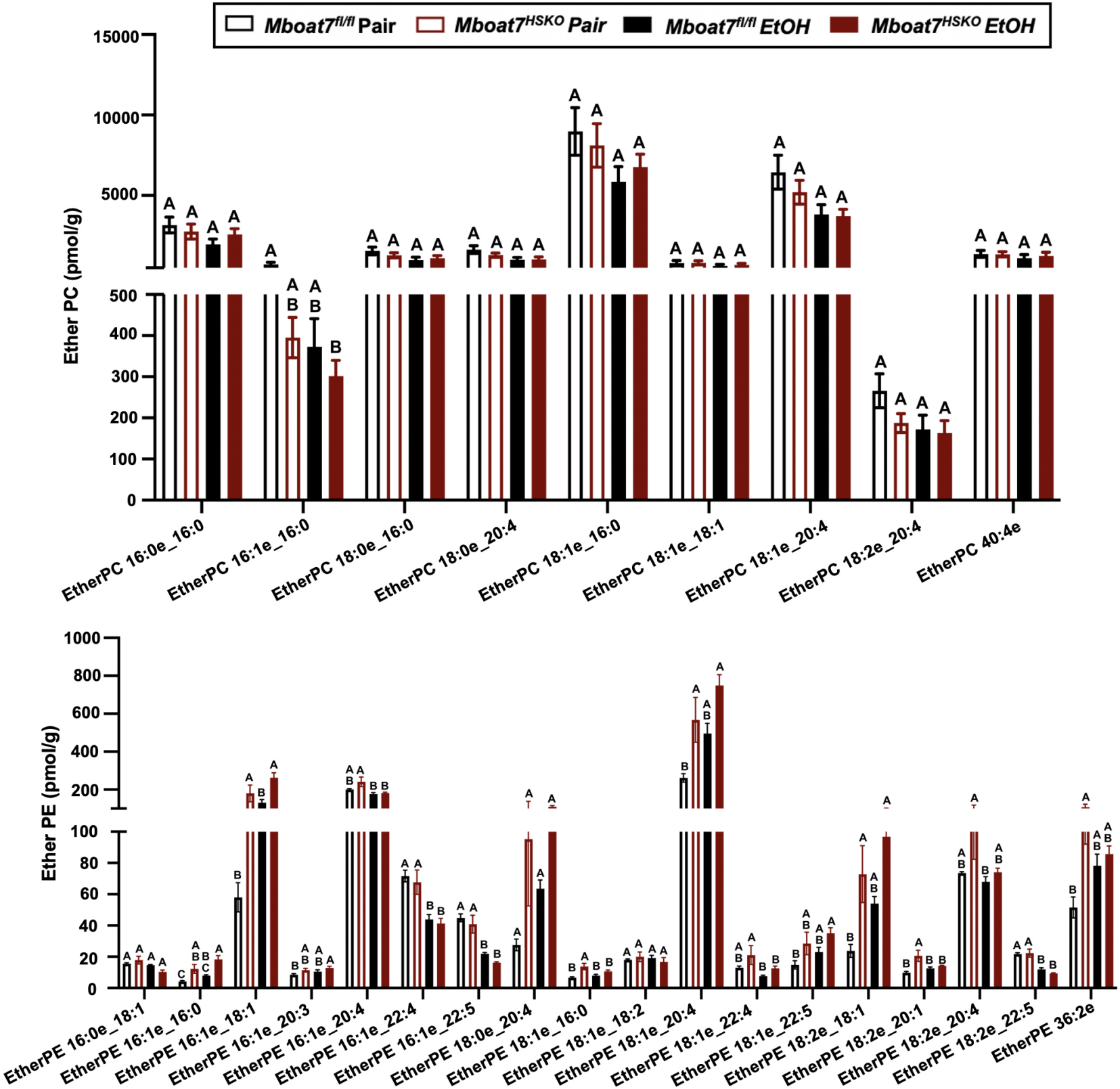
Mboat7fl/fl Pair
Mboat7HSKO Pair
Mboat7fl/fl EtOH
Mboat7HSKO EtOH
Ether PC (pmol/g)
EtherPC 16:0e_16:0
EtherPC 16:1e_16:0
EtherPC 18:0e_16:0
EtherPC 18:0e_20:4
EtherPC 18:1e_16:0
EtherPC 18:1e_18:1
EtherPC 18:1e_20:4
EtherPC 18:2e_20:4
EtherPC 40:4e
Ether PE (pmol/g)
EtherPE 16:0e_18:1
EtherPE 16:1e_16:0
EtherPE 16:1e_18:1
EtherPE 16:1e_20:3
EtherPE 16:1e_20:4
EtherPE 16:1e_22:4
EtherPE 16:1e_22:5
EtherPE 18:0e_20:4
EtherPE 18:1e_16:0
EtherPE 18:1e_18:2
EtherPE 18:1e_20:4
EtherPE 18:1e_22:4
EtherPE 18:1e_22:5
EtherPE 18:2e_18:1
EtherPE 18:2e_20:1
EtherPE 18:2e_20:4
EtherPE 18:2e_22:5
EtherPE 36:2e

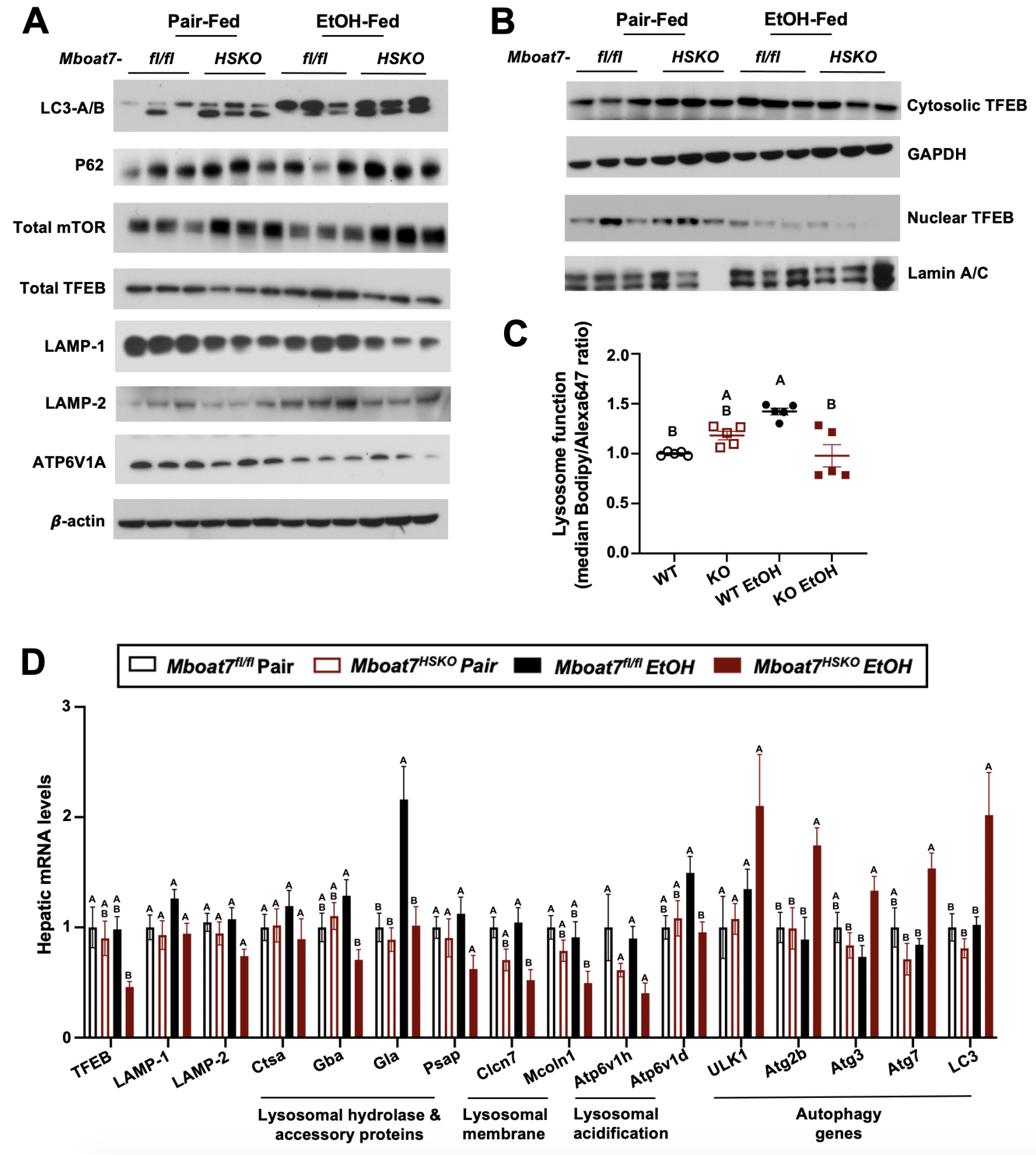
A
Pair-Fed
EtOH-Fed
Mboat7-
fl/fl
HSKO
fl/fl
HSKO
LC3-A/B
P62
Total mTOR
Total TFEB
LAMP-1
LAMP-2
ATP6V1A
β-actin
B
Pair-Fed
EtOH-Fed
Mboat7-
fl/fl
HSKO
fl/fl
HSKO
Cytosolic TFEB
GAPDH
Nuclear TFEB
Lamin A/C
C
Lysosome function
(median Bodipy/Alexa647 ratio)
2.0
1.5
1.0
0.5
0.0
WT
KO
WT EtOH
KO EtOH
D
Mboat7fl/fl Pair
Mboat7HSKO Pair
Mboat7fl/fl EtOH
Mboat7HSKO EtOH
Hepatic mRNA levels
3
2
1
0
TFEB
LAMP-1
LAMP-2
Ctsa
Gba
Gla
Psap
Clcn7
Mcoln1
Atp6v1h
Atp6v1d
ULK1
Atg2b
Atg3
Atg7
LC3
Lysosomal hydrolase & accessory proteins
Lysosomal membrane
Lysosomal acidification
Autophagy genes

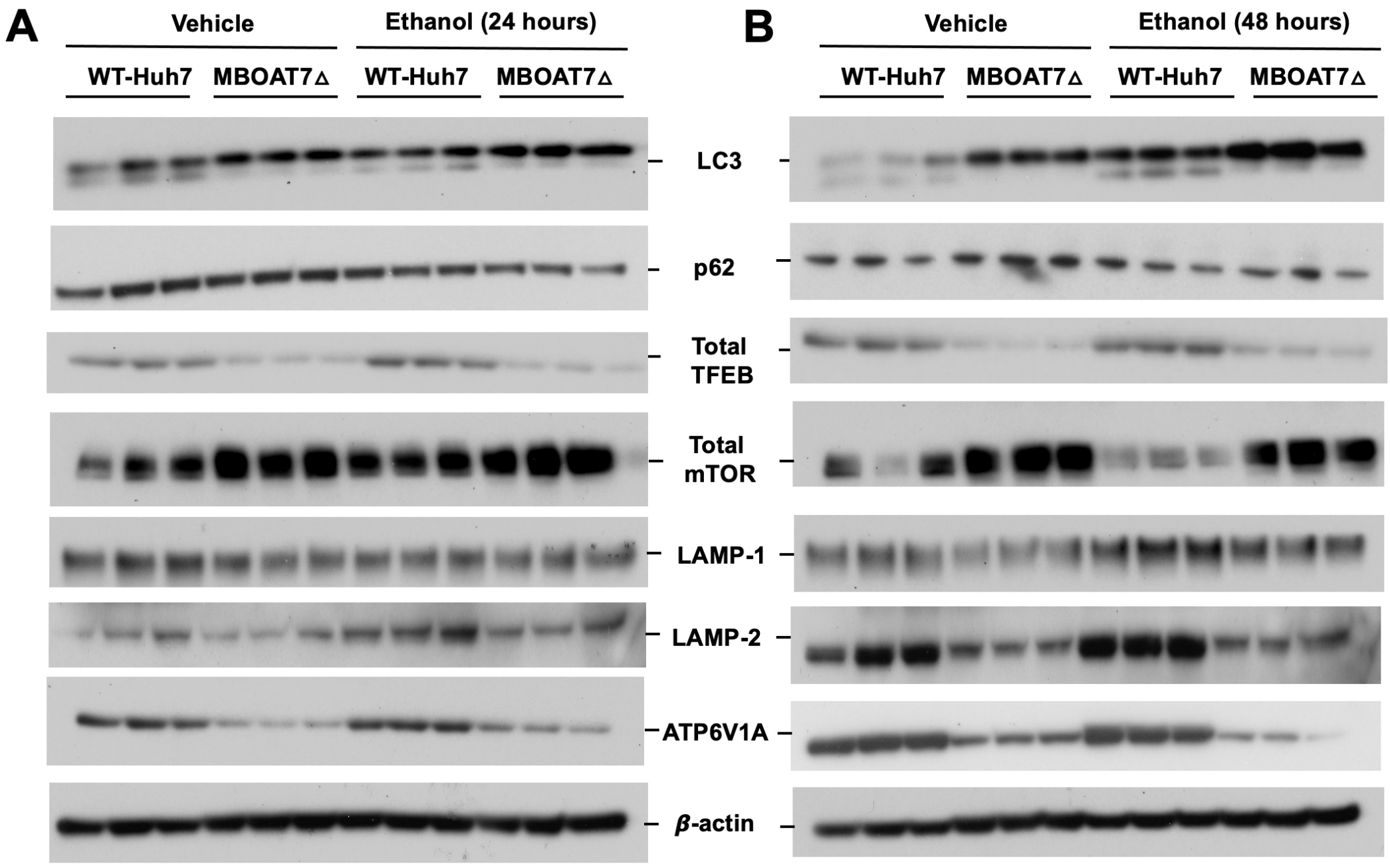
A
Vehicle
Ethanol (24 hours)
WT-Huh7
MBOAT7Δ
WT-Huh7
MBOAT7Δ
B
Vehicle
Ethanol (48 hours)
WT-Huh7
MBOAT7Δ
WT-Huh7
MBOAT7Δ
LC3
p62
Total TFEB
Total mTOR
LAMP-1
LAMP-2
ATP6V1A
β-actin

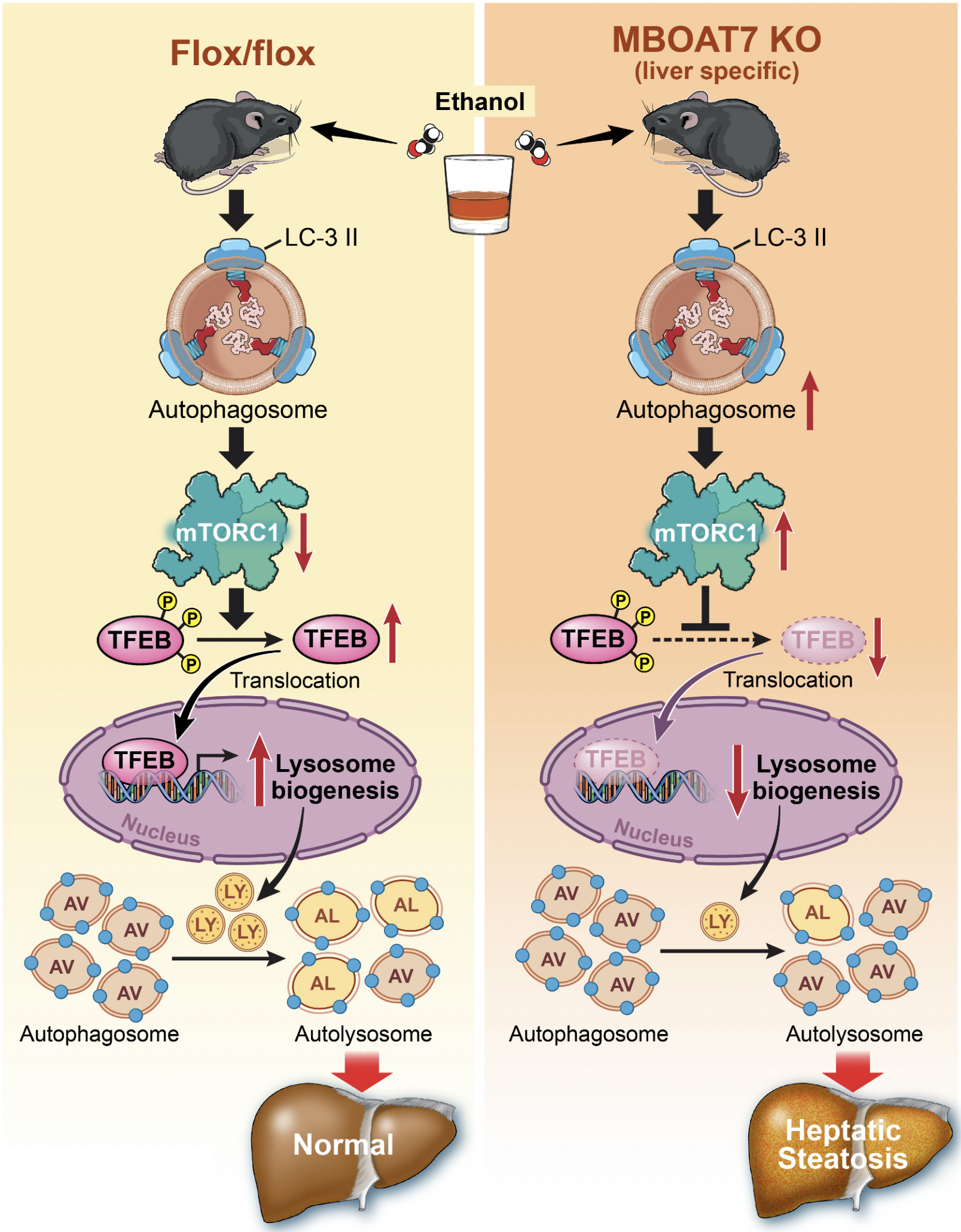
Flox/flox
MBOAT7 KO
(liver specific)
Ethanol
LC-3 II
Autophagosome
mTORC1
TFEB
P
Translocation
Lysosome
biogenesis
Nucleus
AV
LY
AL
Autophagosome
Autolysosome
Normal
Heptatic
Steatosis